BIOCHEMISTRY
including biophysical chemistry & molecular biology

ARTICLE

pubs.acs.org/biochemistry

Identification of in Vitro Autophosphorylation Sites and Effects of Phosphorylation on the *Arabidopsis* CRINKLY4 (ACR4) Receptor-like Kinase Intracellular Domain: Insights into Conformation, Oligomerization, and Activity

Matthew R. Meyer,[†] Cheryl F. Lichti,[‡] R. Reid Townsend,[‡,§] and A. Gururaj Rao*[,†]

[†]Department of Biochemistry, Biophysics and Molecular Biology, Iowa State University, Ames, Iowa 50011, United States

[‡]Department of Medicine, Washington University School of Medicine, 660 South Euclid Avenue, St. Louis, Missouri 63130, United States

[§]Departments of Medicine, Cell Biology and Physiology, Washington University School of Medicine, 660 South Euclid Avenue, St. Louis, Missouri 63130, United States

ABSTRACT: *Arabidopsis* CRINKLY4 (ACR4) is a receptor-like kinase (RLK) that consists of an extracellular domain and an intracellular domain (ICD) with serine/threonine kinase activity. While genetic and cell biology experiments have demonstrated that ACR4 is important in cell fate specification and overall development of the plant, little is known about the biochemical properties of the kinase domain and the mechanisms that underlie the overall function of the receptor. To complement *in planta* studies of the function of ACR4, we have expressed the ICD in *Escherichia coli* as a soluble C-terminal fusion to the N-utilization substance A (NusA) protein, purified the recombinant protein, and characterized the enzymatic and conformational properties. The protein autophosphorylates via an intramolecular mechanism, prefers Mn^{2+} over Mg^{2+} as the divalent cation, and displays typical Michaelis−Menten kinetics with respect to ATP with an apparent K_m of 6.67 ± 2.07 μM and a V_{max} of 1.83 ± 0.18 nmol min^{-1} mg^{-1}. Autophosphorylation is accompanied by a conformational change as demonstrated by circular dichroism, fluorescence spectroscopy, and limited proteolysis with trypsin. Analysis by nanoliquid chromatography and mass spectrometry revealed 16 confirmed sites of phosphorylation at Ser and Thr residues. Sedimentation velocity and gel filtration experiments indicate that the ICD has a propensity to oligomerize and that this property is lost upon autophosphorylation.

A fundamental challenge in the developmental biology of higher organisms is striking a balance among cell proliferation, differentiation, and specification so they can undergo proper organogenesis and development. In mammalian systems, receptor tyrosine kinases (RTKs), such as the members of the epidermal growth factor (EGF) receptor family, represent a class of proteins that perceive and regulate inter- and intracellular processes pertaining to stem cell proliferation and differentiation.[1,2] The architecture of RTKs consists of an extracellular ligand binding domain, a transmembrane helix, and an intracellular kinase domain. In the classic example, members of the EGF receptor family undergo ligand-induced homo- or heterodimerization, followed by intracellular kinase activation via trans phosphorylation.[3,4] Homo- or heterodimerization regulates which downstream signaling pathways are activated through phosphorylation of specific tyrosine residues and recruitment of specific intracellular substrates in response to differential ligand binding.[3,5,6] Mounting evidence, as in the case of the well-characterized Brassinosteroid pathway and the *CLAVATA* (*CLV*) pathway, supports the occurrence of ligand-induced, receptor-mediated signaling involved in plant development similar to RTK signaling in mammalian systems.[7,8] Although >400 putative receptor-like kinases (RLKs) have been identified in the *Arabidopsis* genome, only a few have been characterized in detail.[9,10]

First described as a growth factor-like receptor in maize, CRINKLY4 (CR4) is a RLK involved in the proper formation of the epidermal layer in the leaves and the aleurone monolayer in the kernel.[11,12] The protein consists of an extracellular domain with seven repeating regions (each with 39 amino acids), three cysteine-rich regions that are similar to the extracellular motifs of the tumor necrosis factor receptor, a single transmembrane-spanning region, and an active intracellular serine/threonine kinase domain.[11,13,14] An ortholog in *Arabidopsis*, ACR4, contains all the architectural features of maize CR4 and functions in a similar manner. ACR4 primarily affects epidermal cell

Received: December 4, 2010
Revised: February 3, 2011
Published: February 04, 2011

Table 1. Primers Used in Cloning and Mutagenesis Experiments

primer	mutation	sequence (5′ → 3′)
1	−	GTGGTGGTGGATCCGAGGTACAGATTGAGGAATTG
2	−	GCGCGTCGACTCAGAAATTATGATGCAAG
3	K540A	CCACTGTTGCAGTGGCGAGAGCGATAATGTC
4	D641A	CTCCCGTGATTCACCGGGCCATTAAATCATCAAACATTC
5	S663A	GCTGATTTTGGTCTCGCCTTACTTGGTCCTGTCG
6	S670A	CTTGGTCCTGTCGATGCCGGCTCTCCTTTGGC
7	S672A	CCTGTCGATAGCGGCGCTCCTTTGGCAGAAC
8	T681A	GAACTACCAGCAGGAGCTCTCGGTTACCTTG
9	Y684F	GCAGGAACTCTCGGTTTCCTTGATCCCGAGTAC
10	T681D	GAACTACCAGCAGGAGATCTCGGTTACCTTG
11	Y684D	GCAGGAACTCTCGGTGACCTTGATCCCGAGTAC
12	Y684S	GCAGGAACTCTCGGTTCCCTTGATCCCGAGTAC
13	Y684T	GCAGGAACTCTCGGTACCCTTGATCCCGAGTAC
14	S663D	GCTGATTTTGGTCTCGACTTACTTGGTCCTGTCG
15	S670D	CTTGGTCCTGTCGATGACGGCTCTCCTTTGGC
16	S672D	CCTGTCGATAGCGGCGATCCTTTGGCAGAAC

morphology in the ovules and sepal margins of the plant, is required for proper morphogenesis of developing embryos, and is necessary for the proper formation of the epidermal layer in leaves. Seeds from *acr4* plants show defects in seed coat development and loss of epidermal and cuticle formation, leading to fusion of tissues.[14−17] Recently, ACR4 has been described as a regulator of columella stem cell differentiation in the root apical meristem and lateral root formation in the developing root.[18,19] Loss of ACR4 function results in the proliferation of columella stem cells, and a module involving interactions between the CLE40 peptide, ACR4, and a homeobox transcription factor, WOX5, has been proposed as a signaling mechanism that is similar to the CLV signaling pathway that mediates stem cell proliferation and differentiation in the apical meristem.[19]

Thus, ACR4 is a RLK whose functions are critical to the development of virtually the entire plant.[15−19] Importantly, while genetic and cell biology studies have made it apparent that the RLK is important in cell fate specification, there is little or no knowledge of the biochemical basis of its function and its involvement in regulatory networks. In vitro biochemical and biophysical studies of recombinant proteins can often provide valuable clues for understanding in vivo physiological functions. Indeed, detailed structural and mechanistic studies on a number of recombinantly expressed receptor kinase domains in both animal and plant systems have not only facilitated the development of useful biochemical models for validating in vivo functions but also fostered the development of various protein probes for the dissection of signaling pathways and isolation of interacting proteins. However, such studies require adequate amounts of soluble protein. To this end, we have successfully expressed milligram quantities of the intracellular domain (ICD) of ACR4 in fusion with the NusA protein in an *Escherichia coli* system. We have characterized the autophosphorylation activity, mapped the autophosphorylation sites by mass spectrometry, and demonstrated that the RLK is a member of the RD family of kinases.

MATERIALS AND METHODS

Construction of the ACR4 Intracellular Domain (ICD) Expression Plasmid. The ACR4 intracellular domain, termed JKC (residues 456−895), was cloned into the pET-44b(+) plasmid (Novagen) that encodes an N-terminal NusA fusion tag, two six-His tags, a thrombin cleavage site, and an enterokinase cleavage site. The ACR4 JKC was PCR amplified with primer 1 and primer 2 (Table 1), cloned between the BamHI and SalI restriction sites, and verified by DNA sequencing. The plasmid, termed pNusA:JKC, was used for subsequent protein expression.

Preparation of the kinase inactive mutant plasmid was completed using the QuickChange Multi Site-Directed Mutagenesis Kit (Stratagene) by introducing point mutations into the pNusA:JKC plasmid at codons encoding residues required for kinase activity. Mutagenic primer 3 mutated lysine 540 to alanine (K540A), and primer 4 mutated the catalytic aspartate 641 to alanine (D641A). The plasmid, termed pNusA:JKC2m, was subsequently used for expression of the kinase inactive form of the ACR4 ICD, JKC2m. Activation loop mutations were similarly made using mutagenic primers 5−16 listed in Table 1.

Protein Expression and Purification of NusA-Fused ACR4 JKC Proteins. The ACR4 JKC was expressed as a C-terminal fusion to the NusA solubility tag. Plasmids were transformed into chemically competent BL21(DE3) pLysS (Promega) *E. Coli* cells. A 500 mL culture was supplemented with ampicillin (100 μg/mL) and grown at 37 °C, with shaking, to an OD_{600} of 0.6−0.8. The temperature was then reduced to 20 °C and protein expression induced with isopropyl 1-thio-β-D-galactopyranoside (IPTG) to a final concentration of 1 mM. After being incubated for 6 h, the cells were harvested by centrifugation, and the cell pellet was used immediately. The pellet was resuspended in 10 mL of lysis buffer [1× TBS (pH 7.5), 50 mM imidazole, 1% Triton X-100, and 1 mM DTT] and supplemented with AEBSF (final concentration of 1 mM). The cell suspension was sonicated to release soluble fusion protein, and the resulting lysate was centrifuged in a microcentrifuge at maximal speed for 25 min at 4 °C. The lysate was then incubated for 1 h at 4 °C in batch mode with a 0.5 mL bed volume of Ni^{2+} IMAC Sepharose High Performance resin (GE Healthcare) equilibrated with lysis buffer. After incubation, the lysate/resin mixture was added to a 10 mL disposable chromatography column and the unbound material was allowed to flow through it. The resin was then washed with 10 mL of wash buffer [1× TBS (pH 7.5), 50 mM imidazole, 0.1% Triton X-100, and 1 mM DTT], and bound protein was successively eluted with 2 mL of elution buffer

[50 mM Tris-HCl (pH 8.0), 150 mM NaCl, 150 mM imidazole, and 1 mM DTT]. The final concentration of metal affinity-purified protein at this stage is typically greater than 6 mg/mL.

A secondary gel filtration step was used to purify the NusA fusion proteins using an ÄKTA FPLC system (Amersham). The metal affinity-enriched fusion proteins were passed through a Superdex G200 Global 10/30 column (GE Healthcare) equilibrated with column buffer [50 mM Tris-HCl (pH 8.0), 150 mM NaCl, and 1 mM DTT]. Peak fractions corresponding to the fusion protein were collected, pooled, and concentrated. The resulting purified proteins were used in further experiments.

Purification of JKC Proteins without Tags. The affinity-enriched protein sample (as described above) was treated with 1 unit of restriction grade thrombin (Novagen) per 3.5 mg for 20 min at room temperature. The cleavage reaction mixture was then loaded onto a MonoQ Global 10/50 column (GE Healthcare) equilibrated with anion-exchange buffer [50 mM Tris-HCl (pH 8.0) and 1 mM DTT]. Cleaved ACR4 JKC was eluted off the column by gradient elution with anion elution buffer [50 mM Tris (pH 8.0), 1 M NaCl, and 1 mM DTT]. According to the ExPASy Proteomics Server, the calculated pI of the NusA tag is 4.83 and that of the JKC is 6.47. Peak fractions corresponding to the ACR4 JKC were collected, pooled, and concentrated. The resulting purified proteins were used in subsequent experiments. Note that after cleavage the ACR4 JKC recombinant protein contains 20 extraneous amino acids encoded by the pET-44b(+) vector at the N-terminus.

Antibodies. Polyclonal antibodies to the JKC protein were raised at the Hybridoma Facility at Iowa State University by repeated immunizations of rabbits with the highly purified antigen, and purified IgG was prepared from whole serum by affinity chromatography. The monoclonal antibody to the NusA tag was purchased from Novagen (EMD Chemicals, Gibbstown, NJ). This antibody specifically detects fusion proteins containing the NusA tag sequence expressed with the pET-44 vector series.

Circular Dichroism (CD) Measurements. JKC purified from *E. Coli* (naïve JKC), autophosphorylated JKC (pJKC), and JKC2m were dialyzed overnight at 4 °C in 10 mM Tris-HCl (pH 7.4) and 0.1 mM TCEP and concentrated to an A_{280} value of approximately 1.0. Far-UV spectra of each protein were recorded with a Jasco J-710 spectropolarimeter, in a 0.1 cm path length cuvette with excitation wavelengths ranging from 190 to 260 nm.

Fluorescence Measurements. Naïve JKC, JKC2m, and pJKC were dialyzed in 10 mM Tris-HCl (pH 7.4) and 0.1 mM TCEP and brought to an A_{280} of 0.1 prior to fluorescence scans. Measurements were taken in a 1 cm cuvette at room temperature with a Cary Eclipse spectrofluorimeter (Varian). Scans were executed at an excitation wavelength of 280 nm, a bandwidth of 5 nm, and a scan speed of 120 nm/min.

Kinase Activity Assays. The optimal buffer condition for kinase activity was determined to include 20 mM Bis-Tris (pH 7.2), 25 mM NaCl, 5 mM $MnCl_2$, 1 mM DTT, 25 μM ATP, and a temperature of 30 °C. This was established by performing individual reactions with 2 μg of NusA:JKC protein incubated under varying buffer conditions, including Mn^{2+} (0.05−50 mM), ATP (1−50 μM), DTT (0−10 mM), and NaCl (0−300 mM), in the pH range of 5.8−8.8. All reactions were conducted in a 20 μL volume in the presence of 5 μCi of [γ-^{32}P]ATP (6000 Ci/mmol, Perkin-Elmer) and mixtures incubated for 1 h at room temperature. Reactions were terminated by addition of 6 μL of 4× Laemmli buffer and mixtures boiled for 5 min. Proteins were resolved by 10% SDS−PAGE, and gels were stained with Coomassie Brilliant Blue R-250 and then analyzed by exposure to an autoradiograph film or a phosphorimaging screen.

Assays for determining the autophosphorylation mechanism were performed using the NusA:JKC and JKC proteins. A series of reactions including increasing concentrations of NusA:JKC in the range of 0.2−3.4 μM (or up to ∼2.4 μM in the case of JKC) were conducted. The protein was incubated in 20 μL reaction mixtures of optimized kinase buffer containing 2.5 μCi of [γ-^{32}P]ATP. Reactions were initiated via the addition of the enzyme and mixtures incubated for 15 min at room temperature. The reactions were then terminated and mixtures treated as described above. Protein bands were excised from the gel, and radioactivity was determined by scintillation counting. The extent of incorporation of phosphate for each sample was calculated on the basis of the radioactive counts and the use of a [γ-^{32}P]ATP standard curve. The data were then used to generate a van't Hoff plot (the logarithm of the enzyme activity vs the logarithm of the enzyme concentration), and the intramolecular nature of the mechanism was inferred from the slope of this plot. Kinetic data were fit using the Sigma Plot 11.2 (Systat Software Inc., San Jose, CA) Enzyme Kinetics module (version 1.3) to determine Michaelis−Menten constants by nonlinear regression analysis.

In a parallel experiment, autophosphorylation assays were also performed independently with naïve NusA:JKC, JKC2m, or both proteins incubated together. Incubations of the NusA tag alone or with either protein were used as controls for the assay. Each reaction was conducted with 2 μg of protein in optimized kinase buffer containing 5 μCi of [γ-^{32}P]ATP. Reactions were allowed to proceed for 1 h at room temperature and mixtures processed as described above. To determine if the kinase could phosphorylate other exogenous substrates, we incubated naïve NusA:JKC with 2 μg of myelin basic protein (MyBP) and conducted the phosphorylation reaction as described above.

Analysis of Phosphorylation Status. Two techniques were utilized to determine the phosphorylation status of JKC2m, naïve JKC, and pJKC. One approach utilized the phosphoprotein stain Pro-Q Diamond (Invitrogen). Approximately 1 μg of each protein was separated via 12% SDS−PAGE. The gel was first fixed for 2 × 30 min with a solution containing 50% methanol and 10% acetic acid and then washed three times with deionized water. It was then stained with Pro-Q Diamond for 90 min in the dark and then destained using 50 mM sodium acetate buffer (pH 4.0) containing 20% acetonitrile. Images of the stained gel were acquired on a Molecular Dynamics Typhoon scanner (Amersham Biosciences) with a 532 nm laser for an excitation source and a 580 nm bandpass emission filter.

In the second approach, phosphorylation was assessed by Western blot analysis using a polyclonal, anti-phosphothreonine antibody (Cell Signaling Technology, #3981). Briefly, ∼1 μg of each protein was separated via 12% SDS−PAGE followed by blotting to a PVDF membrane. The membrane was blocked, probed with the primary antibody (1:1000), washed, and then probed with a secondary anti-rabbit IgG antibody (1:30000) conjugated to alkaline phosphatase (Sigma). Protein detection was completed using an AP Conjugate Substrate kit (Bio-Rad).

Sample Preparation for Liquid Chromatography−Tandem Mass Spectrometry (LC−MS/MS) Analysis. To prepare peptides, we concentrated the proteins by TCA precipitation and resuspended them in 4 M urea in 50 mM NH_4HCO_3 (pH 7.8). Proteins were reduced with 10 mM TCEP for 30 min at 50 °C followed by

alkylation with 20 mM iodoacetamide for 30 min at room temperature in the dark; 50 mM NH_4CO_3 (pH 7.8) was added to the sample to dilute urea to <1 M. The protein was then digested with 1:50 (w/w, enzyme to substrate) sequencing grade modified trypsin (Promega) overnight at 37 °C. The resulting peptides were desalted on a SOURCE 15 RPC column (GE Healthcare) and eluted in 90% acetonitrile and 0.1% TFA. The eluted peptides were then dried down in a vacuum centrifuge. Phosphopeptides were enriched using the PHOS-Select Ga^{3+} Silica Spin Column kit (Supelco) according to its instructions.

Peptides were eluted into autosampler vials with 60% acetonitrile in 1% formic acid. The quality of the peptide digests was assessed using MALDI-TOF mass spectrometry. The remaining sample was dried, dissolved in 25 μL of an aqueous acetonitrile/formic acid mixture (1%/1%), and analyzed by high-resolution nanoliquid chromatography and mass spectrometry (nano-LC−MS).

High-Resolution Mass Spectrometry. The complex peptide mixtures were analyzed using high-resolution nano-LC−MS on a hybrid mass spectrometer consisting of a linear quadrupole ion trap and an Orbitrap (LTQ-Orbitrap XL, Thermo Fisher Scientific). Chromatographic separations were performed using a NanoLC-1D Plus instrument (Eksigent) for gradient delivery and a cHiPLC-nanoflex instrument (Eksigent) containing a 15 cm × 75 μm C18 column (ChromXP C18-CL, 3 μm, 120 Å, Eksigent). The liquid chromatograph was interfaced to the mass spectrometer with a nanospray source (PicoView PV550, New Objective). The mobile phases were 1% formic acid in water (solvent A) and 1% formic acid in acetonitrile (solvent B). After equilibration of the column in 98% solvent A and 2% solvent B, the samples (5 μL) were injected from vials using the LC-system autosampler at a flow rate of 500 nL/min. The peptides were eluted at 250 nL/min with the following gradient: isocratic at 2% B from 0 to 3 min, from 2 to 50% B from 3 to 73 min, from 50 to 80% B from 73 to 83 min, isocratic at 80% B from 83 to 86 min, from 80 to 2% B from 86 to 87 min, and isocratic at 2% B from 87 to 102 min. The total run time, including column equilibration, sample loading, and analysis, was 128 min. The survey scans (m/z 350−2000) (MS1) were acquired at high resolution (60000 at m/z 400) in the Orbitrap, and the MS/MS spectra (MS2) were acquired in the linear ion trap at low resolution, both in profile mode. The maximal injection times for the MS1 scan in the Orbitrap and the LTQ were 50 and 100 ms, respectively. The automatic gain control targets for the Orbitrap and the LTQ were 5×10^5 and 3×10^4, respectively. The MS1 scans were followed by six MS2 events in the linear ion trap with collision activation in the ion trap (parent threshold of 1000, isolation width of 2.0 Da, normalized collision energy of 30%, activation Q of 0.250, and activation time of 30 ms). Dynamic exclusion was used to remove selected precursor ions (−0.20/1.0 Da) for 90 s after MS2 acquisition. A repeat count of 1, a repeat duration of 45 s, and a maximal exclusion list size of 500 were used. The following ion source parameters were used: capillary temperature of 200 °C, source voltage of 3.5 kV, source current of 100 μA, capillary voltage of 33 V, and the tube lens at 120 V. The data were acquired using *X*calibur, version 2.0.7 (Thermo Fisher). For high-resolution targeted analysis, the parent ions from an inclusion m/z list within a retention time window were selected for acquisition of peptide fragmentation spectra at 7500 resolution. MS/MS spectral acquisition was triggered with an isolation width of 4 Da when the signal for the ion of interest exceeded 10000 counts. The maximal injection times for the MS1 scan in the Orbitrap and the LTQ were both 500 ms, and the maximal injection times for the MS*n* scan in the Orbitrap and the LTQ were 750 and 1000 ms, respectively. The automatic gain control targets for the Orbitrap and the LTQ were 2×10^5 and 3×10^4, respectively, for the MS1 scans and 1×10^5 and 1×10^4, respectively, for the MS*n* scans. The MS1 scan was followed by one MS2 event with collision activation in the ion trap (parent threshold of 10000, isolation width of 4.0 Da, normalized collision energy of 30%, activation Q of 0.250, and activation time of 30 ms). The following ion source parameters were used: capillary temperature of 200 °C, source voltage of 3.3 kV, source current of 100 μA, capillary voltage of 34 V, and the tube lens at 125 V.

Data Analysis. The MS2 spectra were analyzed by searching against the ACR4 sequence and expert manual interpretation. The exact masses of the phosphopeptide and fragmentation ions were calculated using the MS-Product utility within Protein Prospector (http://prospector.ucsf.edu). For database searches, the LC−MS files were processed using MASCOT Distiller (Matrix Science, version 2.3.0.0) with the settings previously described.[20] The resulting MS2 centroided files were used for database searching with MASCOT, version 2.1.6, against a custom, in-house database containing ACR4 using the following parameters: trypsin as the enzyme, MS tolerance of 15 ppm, MS/MS tolerance of 0.8 Da with a fixed carbamidomethylation of Cys residues with the variable modifications being oxidation (Met) and phosphorylation (Ser, Thr, and Tyr), a maximal number of missed cleavages of 9, and +1, +2, and +3 charge states. For analysis of the tandem spectra from spectral acquisitions in the Orbitrap (MS2), the raw files were processed using MASCOT Distiller (Matrix Science, Oxford, U.K.) with the following settings: (1) MS processing, 200 data points per dalton, sum aggregation method, maximal charge state of +3, and minimal number of peaks of one; (2) MS/MS processing, 200 data points per dalton, time domain aggregation method, minimal number of peaks of 10, use precursor charge as the maximum; precursor charge and m/z, "try to redetermine charge from the parent scan (tolerance, 1.2 Da)", and one charge default; (3) time domain parameters, minimal number of precursor mass of 300, maximal precursor mass of 16000, precursor m/z tolerance for grouping of 0.01, maximal number of intermediate scans of zero, and minimal number of scans in a group of one; and (4) peak picking, maximal number of iterations of 500, correlation threshold of 0.60, minimal signal-to-noise ratio of 2, minimal peak m/z of 50, maximal peak m/z of 100000, minimal peak width of 0.002, maximal peak width of 0.2, and expected peak width of 0.02. The resulting files were used for database searching with a fragment tolerance of 100 mmu; all other search parameters are identical to those described above.

Analytical Ultracentrifugation. Sedimentation velocity analysis of NusA:JKC, naïve and phosphorylated, was performed on an XL-A analytical ultracentrifuge (Beckman Coulter). The purified protein was dialyzed overnight at 4 °C in 10 mM Tris-HCl (pH 7.4), 50 mM NaCl, and 0.1 mM TCEP. The protein sample was concentrated to an A_{280} of 0.6; 300 μL of the sample was loaded into a preassembled flow-through assembly housing an Epon, two-channel centerpiece and quartz windows. The rotor and sample cell temperatures were allowed to equilibrate to 20 °C for 2 h. The sample was spun at 40000 rpm and 20 °C for a total of 400 scans with a scan rate of one scan per minute. Boundaries were monitored by recording the absorbance at 280 nm. Scan analysis was performed using Van Holde−Weischet

analysis[21] as implemented in Ultrascan 6. Sedimentation coefficients ($S_{20,w}$) were corrected for 20 °C and water.

Limited Proteolysis. The conformational difference between naïve JKC and pJKC proteins was probed by limited proteolysis using trypsin. The naïve protein was purified as described above, and 125 μg of the protein was diluted into a 200 μL volume containing 50 mM Tris-HCl (pH 8.0), 1 mM $CaCl_2$, and 1 mM DTT. Trypsin (Promega) was added at a 1:1000 (w/w) protease:substrate ratio and incubated at room temperature. Aliquots (25 μL) were removed at predetermined time points, and the reaction was stopped by the addition of 6 μL of 4× SDS sample buffer and boiling for 5 min. For pJKC, 125 μg of the protein was first incubated in a 200 μL reaction volume containing 1× kinase buffer and 100 μM ATP for 90 min. Subsequently, 5 μL of 2 M Tris-HCl (pH 8.0) was added to adjust the pH to 8.0 followed by addition of 1 μL of 0.2 M $CaCl_2$ to a final concentration of 1 mM. The digestion reaction was then conducted as described above. Protein samples (~0.5 μg/lane) were separated by 7% SDS−PAGE, and gels were silver stained using the SilverSNAP stain kit from Pierce (Rockford, IL).

RESULTS

Expression, Purification, and Characterization of JKC. The intracellular domain (ICD) of ACR4 (residues 456−895) may be subdivided into the juxtamembrane domain (JM), kinase domain (KD), and carboxy-terminal domain (CTD). Using the NusA protein as the fusion partner, we have expressed and purified milligram quantities of the ICD for biochemical characterization. Figure 1A shows the SDS−PAGE analysis of protein fractions during various steps in the purification of NusA:JKC (lane 3) and JKC (lane 5) from *E. Coli* cells (as described in Materials and Methods). Approximately 6 mg of soluble NusA:JKC and <0.25 mg of JKC were obtained from a 500 mL culture. A similar yield was obtained for the inactive mutant (JKC2m). The identities of the proteins were confirmed by Western blots probed with rabbit polyclonal antibodies raised against the JKC (Figure 1B) and the antibody to the NusA tag (Figure 1C). These blots validate the homogeneity of the protein preparation and demonstrate the absence of copurification of non-full length NusA-tagged proteins. The identity of the purified JKC protein was also confirmed by MALDI-MS analysis of tryptic peptides of the excised protein band (data not shown).

The far-UV CD spectrum of the JKC (Figure 2A) is similar to that reported for other examples of recombinantly expressed kinase domains of receptor tyrosine kinases.[22,23] The three-dimensional structures of several kinase domains show a number of helices, and the observed CD spectrum for naïve JKC (combined with the robust catalytic activity described below) strongly supports the preservation of an ordered structure. Typical α-helical structures display negative bands at 208 and 222 nm. The more negative molar ellipticity value at 208 nm could be attributed to contributions from the juxtamembrane and carboxy-terminal regions of the molecule as well as the 20 extraneous amino acids at the N-terminus encoded by the pET-44b(+) vector (see Materials and Methods). Fluorescence spectroscopy (Figure 2B) shows almost identical profiles for both the mutant and naïve proteins with an emission maximum at 342 nm, consistent with the tryptophan residues being located in similar environments.

Preliminary evidence of the ability of the ICD to oligomerize was obtained during the purification of the metal affinity-enriched

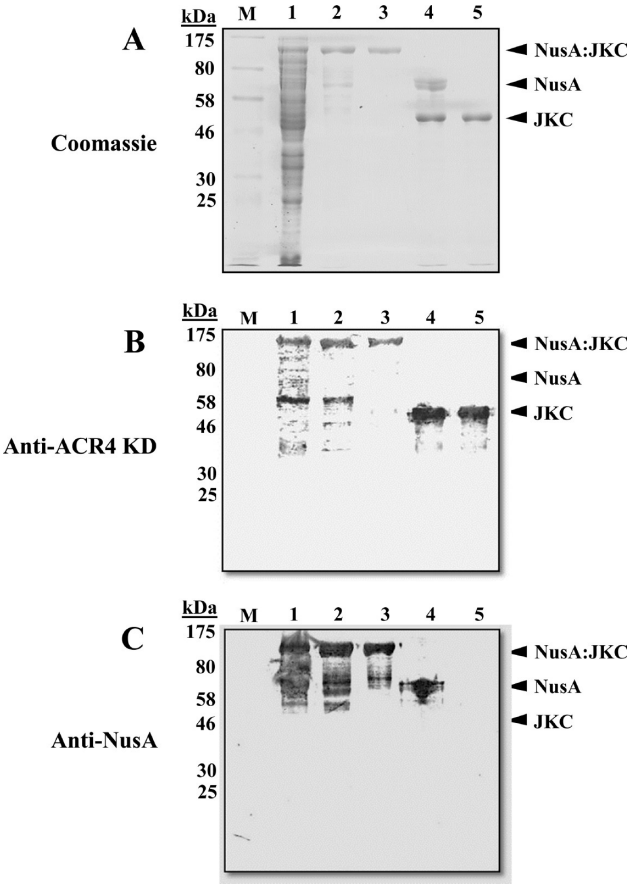

Figure 1. Analysis of protein purification by SDS−PAGE and Western blotting. (A) SDS−PAGE gel (10%) stained with Coomassie blue. (B) Western blot analysis using the polyclonal antibody to the ACR4 kinase domain. (C) Western blot analysis using the monoclonal antibody to the NusA tag. For panels A−C: lane M, molecular weight standards; lane 1, total protein from *E. Coli* lysate; lane 2, affinity-enriched NusA:JKC; lane 3, NusA:JKC purified by gel filtration; lane 4, thrombin-cleaved NusA:JKC; lane 5, JKC purified by anion-exchange chromatography.

NusA:JKC protein by size exclusion chromatography. Typically, at the affinity enrichment step, the protein concentration is >6 mg/mL and is subsequently decreased to ~2 mg/mL (~18 μM) for batchwise purification by gel filtration on a Superdex G200 column. As shown in Figure 3, in addition to eluting as a monomer (peak at a volume of ~12.5 mL), a small proportion of the protein elutes as an aggregate in the void volume. Analysis of these fractions by SDS−PAGE (inset A) indicates that the void volume fraction consists entirely of aggregates of the monomer. An autophosphorylation assay of the aggregate fraction indicated that no kinase activity could be detected in comparison with that of the monomer fraction (inset B). It is also worth noting that the propensity for oligomerization may be concentration-dependent because little or no aggregate is observed in gel filtration experiments at protein concentrations below ~1.5 μM (data not shown).

The self-association of naïve NusA:JKC was also monitored by sedimentation velocity experiments. During sedimentation velocity, homogeneous noninteracting molecules will sediment with discrete sedimentation coefficient (S) values, whereas interacting molecules that lead to higher-order oligomers will exhibit a broad distribution of sedimenting species. Figure 4A shows the percent distribution of species (plotted as diffusion-corrected

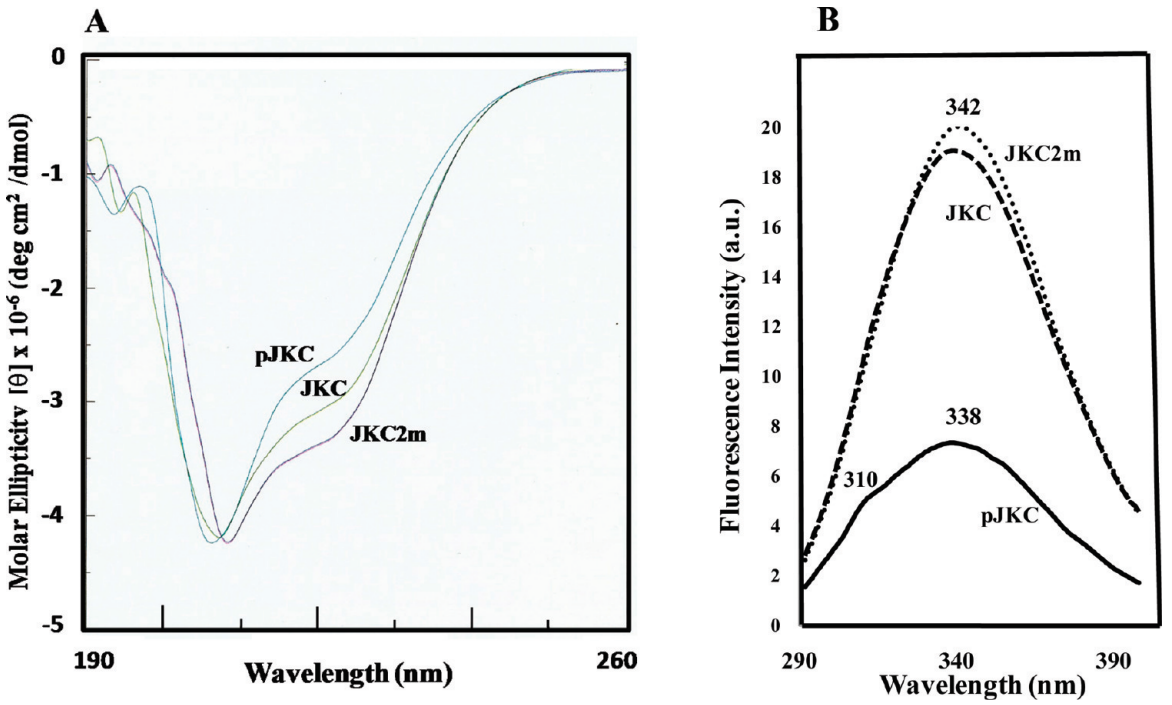

Figure 2. Conformational analysis of JKC proteins. (A) Far-UV CD spectra of inactive JKC2m, naïve JKC, and autophosphorylated pJKC in 10 mM Tris (pH 7.4) and 0.1 mM TCEP with an A_{280} value of ~1.0. (B) Intrinsic fluorescence spectra of JKC2m, JKC, and pJKC in the same buffer with an A_{280} of 0.1. Measurements were taken in a 1 cm cuvette at room temperature with a Cary Eclipse spectrofluorometer (Varian) at an excitation wavelength of 280 nm.

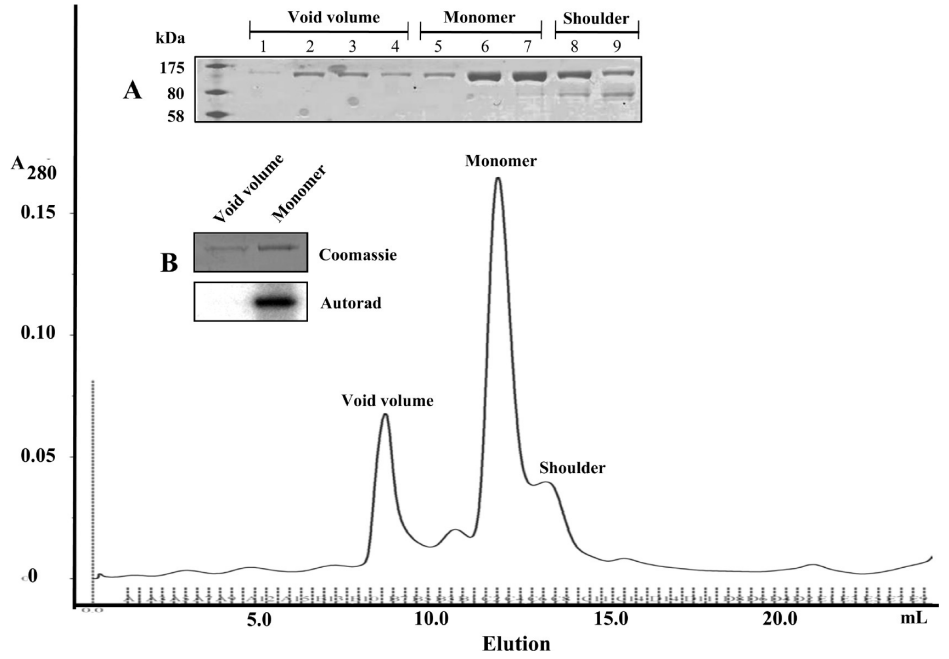

Figure 3. Gel filtration profile of affinity-enriched NusA:JKC in 50 mM Tris (pH 8.0) and 150 mM NaCl during the protein purification scheme. The positions of the aggregate peak in the void volume, the monomer peak, and the shoulder are indicated. (A) SDS−PAGE of void volume (lanes 1−4), monomer (lanes 5−7), and shoulder fractions (lanes 8 and 9). (B) NusA:JKC isolated from the void volume and monomer fractions subjected to an in vitro autophosphorylation assay. NusA:JKC from the monomeric fraction was fully active, whereas NusA:JKC from the void volume fraction had little or no activity.

sedimentation coefficients) along the sedimentation boundary in the velocity sedimentation experiment for naïve NusA:JKC. Approximately 60% of the protein sedimented with an $S_{20,w}$ value of 4, with the remaining 40% showing a considerably wider range of much higher S values, commensurate with association with heterogeneous polymeric species. We also analyzed the data

dx.doi.org/10.1021/bi101935x |*Biochemistry* 2011, 50, 2170–2186

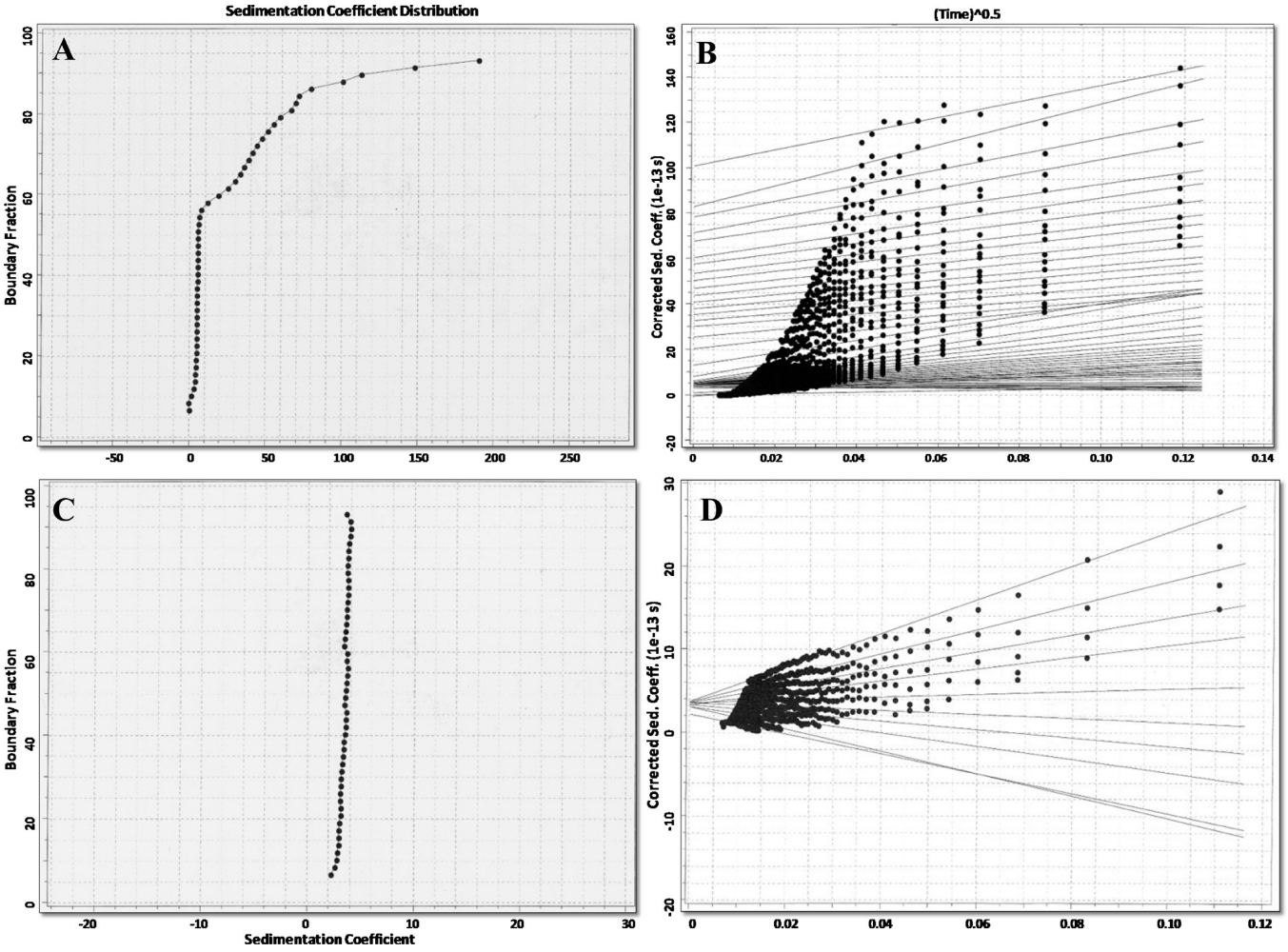

Figure 4. Sedimentation velocity analysis of NusA:JKC (A) and autophosphorylated NusA:JKC (C) performed on an XL-A analytical ultracentrifuge using a protein sample with an A_{280} of 0.6. The sample was spun at 40000 rpm and 20 °C for a total of 400 scans with a scan rate of one scan per minute. (B and D) van Holde−Weischet analysis of NusA:JKC and autophosphorylated NusA:JKC, respectively.

by the Van Holde−Weischet method[21] (Figure 4B). In this analysis, the sedimenting boundary is first divided into a number of segments and the data are fit by linear least-squares analysis to the apparent sedimentation coefficient of each boundary segment. Extrapolation to the *y*-axis then yields the diffusion-corrected sedimentation coefficient for that boundary segment. Typically, a homogeneous sample would be expected to have the same sedimentation coefficient as a function of time in all parts of the boundary, and the extrapolated lines for the various segments should converge to a single value at the *y*-axis.[24] It is also clear by this method of analysis that the naïve protein shows a distinct propensity to aggregate with species with *S* values of >4. The NusA protein is not known to dimerize,[25−28] and we also did not see any evidence of dimerization with the recombinantly expressed NusA protein (data not shown). In contrast, after autophosphorylation, the protein does not aggregate and shows a predominantly homogeneous monomeric species sedimenting with an $S_{20,w}$ value of ∼4 (Figure 4C,D). We were unable to perform sedimentation velocity experiments with the protein without the NusA tag because of the inadequate recovery of soluble protein.

Kinase Activity of NusA:JKC. Interestingly, as observed for some of the other RLKs characterized so far[29−31] the recombinantly expressed ACR4 ICD as a NusA fusion protein prefers Mn^{2+} over Mg^{2+} as the metal ion for autophosphorylation, although the precise physiological significance of this is not obvious. A linear increase in phosphorylation activity is seen with Mn^{2+} concentrations ranging from 0.1 to 5 mM, with maximal activity occurring at 5 mM and quenching at higher concentrations of the metal ion (Figure 5A). A similar linear relationship is seen with Mg^{2+}, but much higher concentrations of Mg^{2+} are required to achieve activity comparable to that with Mn^{2+} as the divalent cation, i.e., 1 mM Mn^{2+} versus 50 mM Mg^{2+} (Figure 5A). This is further illustrated in Figure 5B that shows an autoradiogram of the kinase activity in the presence of 10 mM Mg^{2+}, Mn^{2+}, and Ca^{2+}. No activity is observed with Ca^{2+}, and the activity with Mg^{2+} is significantly lower. In the presence of Mn^{2+}, the reaction is completed in 60 min (for JKC as well) (Figure 5C) at 30 °C at an optimal pH of 7.2 in 20 mM Bis-Tris buffer containing 1 mM DTT and 25 mM NaCl (Figure 5D). The enzyme displays typical Michaelis−Menten kinetics with respect to ATP (Figure 5E), and analysis of the ATP dependence for autophosphorylation by fitting the data to the Michaelis−Menten equation (using the Enzyme Kinetics Module on SigmaPlot 11.2) revealed the K_m and V_{max} values for ATP to be 6.67 ± 2.07 μM and 1.83 ± 0.18 nmol min^{-1} mg^{-1},

dx.doi.org/10.1021/bi101935x |*Biochemistry* 2011, 50, 2170–2186

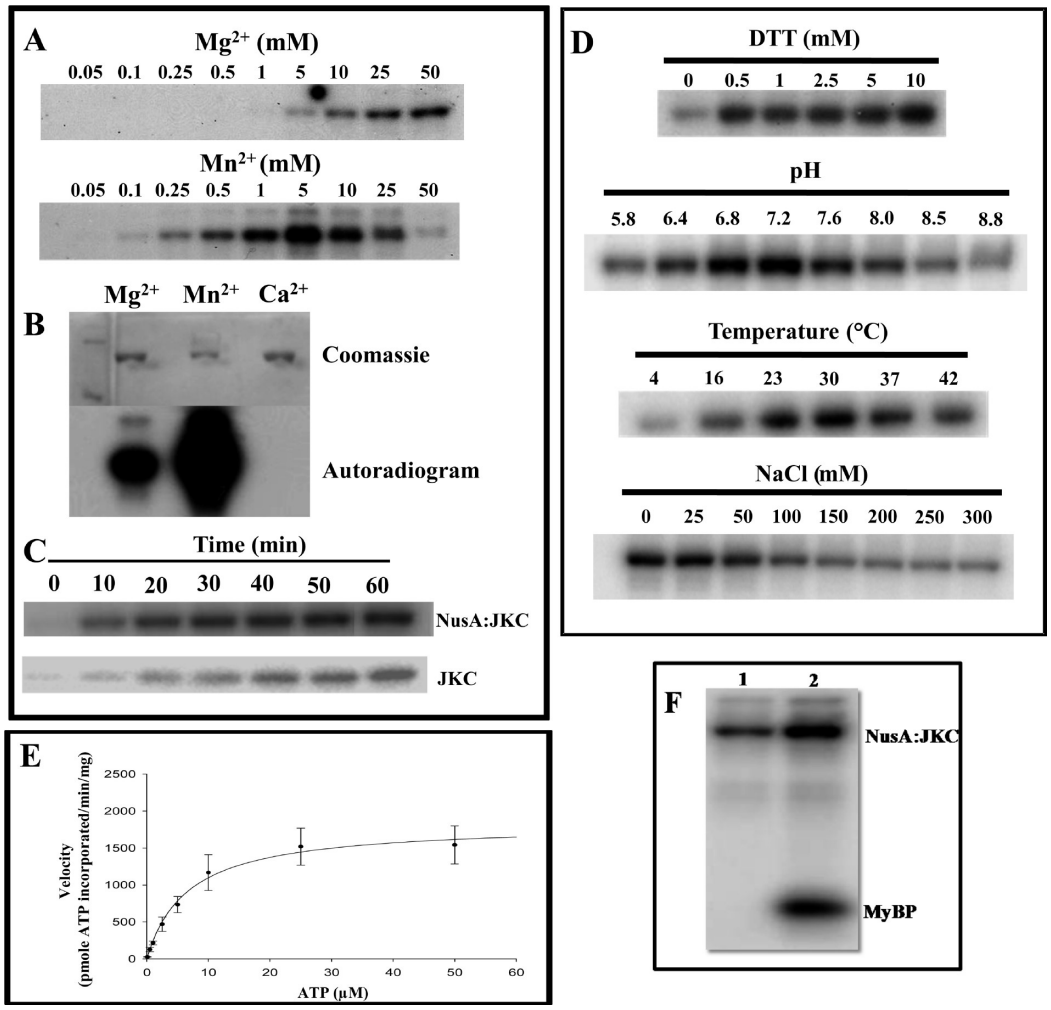

Figure 5. Optimal conditions for in vitro autophosphorylation activity as described in Materials and Methods. Two micrograms of NusA:JKC was incubated in 20 μL of kinase buffer containing 5 μCi of [γ-^{32}P]ATP (6000 Ci/mmol). Reactions were terminated by addition of SDS sample buffer, and proteins were resolved by 10% SDS−PAGE followed by Coomassie Blue staining and phosphorimaging. (A) Concentration dependence of divalent cations. (B) Comparison of 10 mM Mg^{2+}, Mn^{2+}, and Ca^{2+}. (C) Time course of autophosphorylation for NusA:JKC (top) and JKC (bottom). (D) Effect of reducing agent (DTT), pH, temperature, and ionic strength on autophosphorylation. (E) Plot of enzyme velocity vs ATP concentration. Data were fitted directly to the Michaelis−Menten equation using SigmaPlot 11.2 and the Enzyme Kinetics 1.3 module. The K_m value for ATP was 6.67 ± 2.07 μM, and the V_{max} value was 1.83 ± 0.18 nmol min^{-1} mg^{-1}. Data are means ± the standard error (n = 4). (F) NusA:JKC can phosphorylate the exogenous substrate MyBP: lane 1, NusA:JKC; lane 2, NusA:JKC incubated with MyBP.

respectively. The apparent K_m for ATP is also comparable with that observed for other RLKs.[29,30]

Because the native substrate for ACR4 kinase has not yet been determined, we used MyBP as a model substrate in an assay to assess the ability of the kinase to phosphorylate exogenous proteins. As indicated in Figure 5F (lane 2), MyBP is phosphorylated by NusA:JKC.

Autophosphorylation Occurs through an Intramolecular Mechanism. Autophosphorylation reactions of kinases can proceed through either an intramolecular mechanism (first-order with respect to enzyme concentration) or an intermolecular mechanism (second-order with respect to enzyme concentration). We used two approaches to ascertain the mechanism of activity of NusA:JKC. First, we conducted a series of kinase reactions using increasing concentrations of NusA:JKC in the range of 0.1−3.4 μM. As shown in Figure 6A, the rate of autophosphorylation was linear with respect to enzyme concentration and the amount of phosphate incorporation per molecule remained fairly constant over a 2 order of magnitude difference in protein concentration (Figure 6B). The van't Hoff analysis (plot of the logarithm of the phosphorylation rate vs the logarithm of the enzyme concentration, with the value of the slope indicating the order of the reaction) gave a slope of 1.05 ± 0.05 and a correlation coefficient of 0.97 for the linear regression (Figure 6C), suggesting an intramolecular mechanism. Similar results were obtained for assays performed with JKC without the NusA tag (Figure 6D−F), and the van't Hoff plot yielded a slope of ∼1.2 (Figure 6F). Importantly, the lower specific activity of JKC in the concentration range employed (Figure 6E) and the decreased solubility of the protein at higher concentrations attest to the stabilizing influence of the NusA tag on the activity of the enzyme. For further confirmation of the intramolecular mechanism, we performed kinase assays by incubating active NusA:JKC with inactive mutant JKC2m to determine if the latter could be phosphorylated. As shown in Figure 7A, NusA:JKC could undergo autophosphorylation (lane 1) and also phosphorylate the

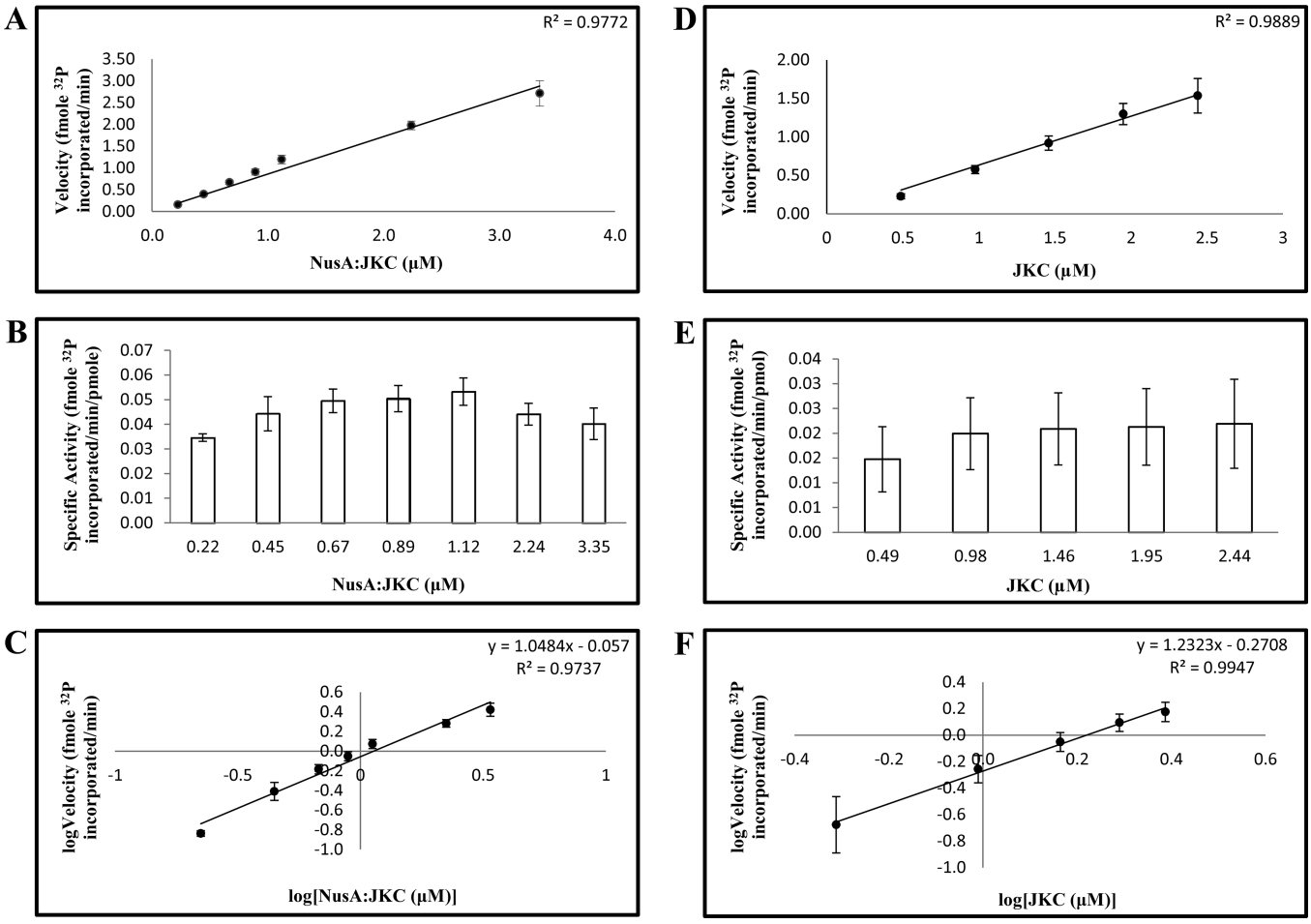

Figure 6. ACR4 autophosphorylates via an intramolecular mechanism. NusA:JKC (A−C) and JKC (D−F) were incubated at increasing enzyme concentrations in an autophosphorylation assay. (A and D) Plot of velocity vs enzyme concentration. (B and E) Plot of specific activity vs enzyme concentration. (C and F) van't Hoff plot of the logarithm of the enzyme velocity vs the logarithm of the enzyme concentration. Linear regression of the data in panels C and F estimates a slope of 1.05 for NusA:JKC and a slope of 1.23 for JKC. All data are means ± the standard error (n = 4).

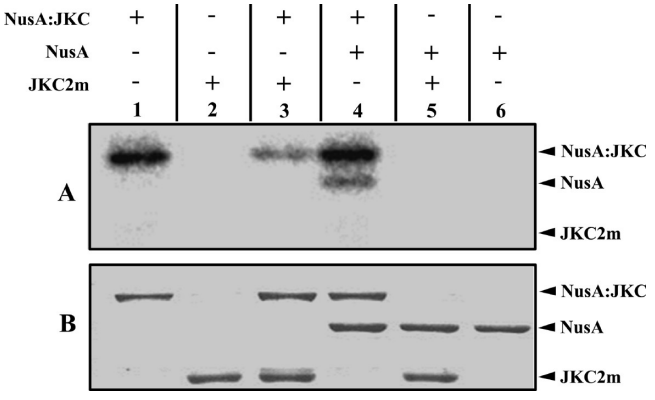

Figure 7. Intramolecular mechanism established by the autophosphorylation assay. Active NusA:JKC and kinase inactive JKC2m were incubated together in an in vitro autophosphorylation assay: lane 1, active NusA:JKC; lane 2, kinase inactive JKC2m; lane 3, active NusA:JKC and inactive JKC2m; lane 4, NusA:JKC and the NusA tag; lane 5, kinase inactive JKC2m and the NusA tag; lane 6, NusA tag. Proteins were resolved by 10% SDS−PAGE and analyzed by phosphorimaging (A) and Coomassie Blue staining (B).

NusA tag (lane 4) but could not phosphorylate the inactive mutant (lane 3). The reduced activity of NusA:JKC in lane 3 may potentially be attributed to the formation of a less active heterodimer between the wild-type and mutant protein. Taken together with the kinetic data, this strongly suggests that the dominant mechanism of autophosphorylation is intramolecular.

Mapping of Autophosphorylation Sites. The datum-dependent tandem mass spectrometric analysis of the tryptic peptides and searching against ACR4 protein sequence revealed several phosphopeptides. The identified phosphopeptides encompassed all the subdomains of the ICD (Figure 8A). Determination of the exact site of phosphorylation within the phosphopeptides was performed by inspection of their fragmentation pattern for specific diagnostic site-determining y_n and b_n ions.[32] As an example, the collisionally induced tandem mass spectrum for phosphopeptide ^{533}DG(pT)TVAVK^{540} is shown in Figure 8B. The most prominent ion is the doubly charged $[M + 2H - 98]^{2+}$ species at m/z 386.71. This is characteristic of a neutral loss of phosphoric acid by which phosphorylation sites are identified. An unambiguous confirmation of Thr^{535} as the phosphorylated residue was afforded by the presence of the phosphorylated b_3 (theoretical m/z of 354.1, observed m/z of

dx.doi.org/10.1021/bi101935x |*Biochemistry* 2011, 50, 2170–2186

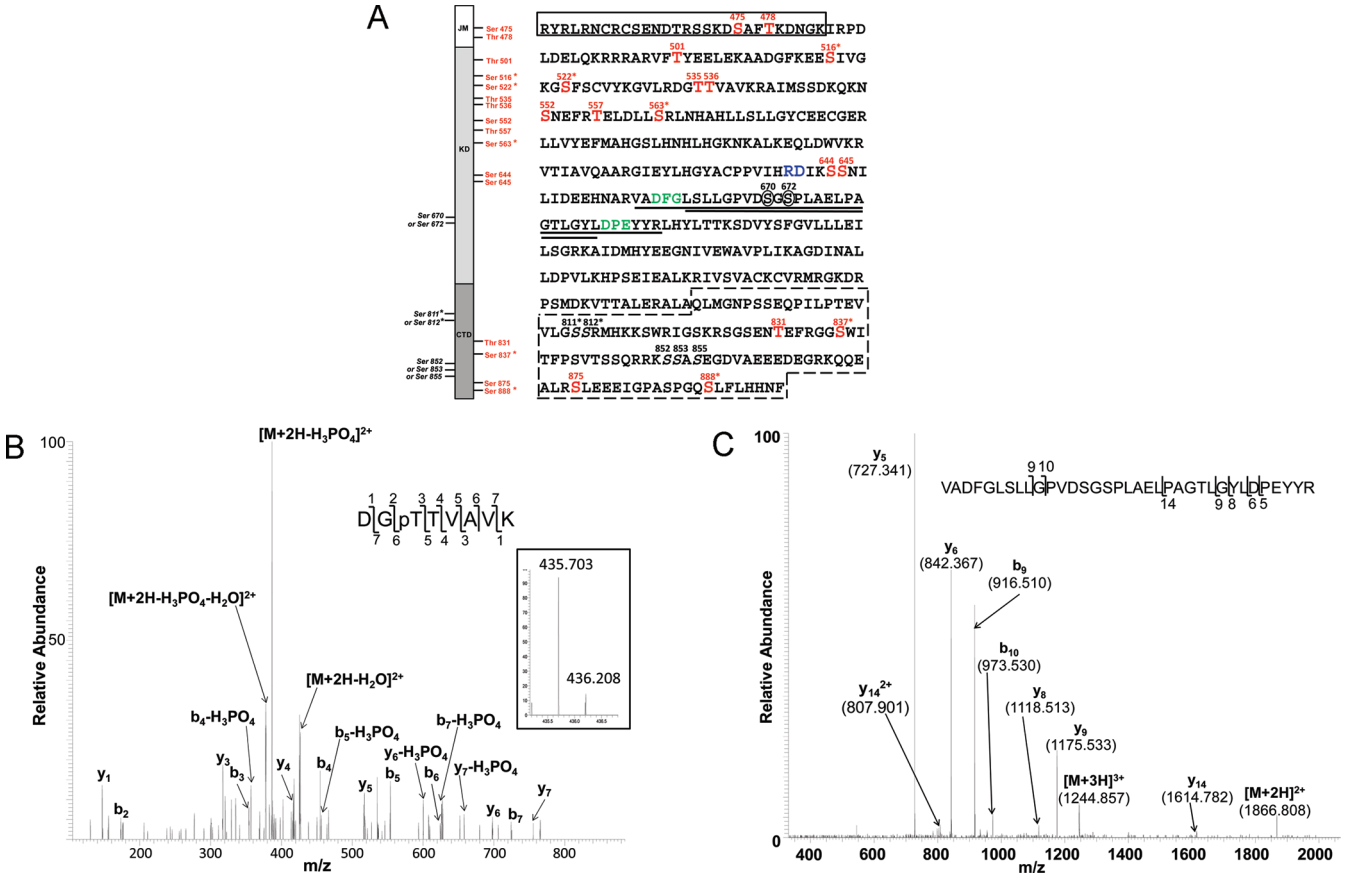

Figure 8. (A) Diagram showing the identified phosphorylation sites. The left panel shows a schematic of the ACR4 ICD showing the boundaries of the JM, KD, and CTD. Confirmed phosphorylated residues in the autophosphorylated protein are colored red and those that are found in the naïve protein denoted with an asterisk. The right panel shows the amino acid sequence of the ICD showing the N-terminal JM region (boxed rectangle), the central KD with the 35-amino acid tryptic peptide (underlined), and the activation loop sequence (doubly underlined) between the DFG and DPE motif (green), the "RD" motif characteristic of RD-type kinases (blue), and the CTD (box with dashed lines). Potential phosphorylation sites are numbered in black, and the two Ser residues (670 and 672) within the activation loop are circled. (B) Collision-induced low-resolution fragmentation spectrum of the phosphopeptide DGpTTVAVK (Mascot ion score of 41), encompassing residues 533−540 of the ACR4 sequence. The presence of phosphorylated b_3 (theoretical m/z of 354.1, observed m/z of 354.1) and y_6 (theoretical m/z of 698.3, observed m/z of 698.2) ions, along with nonphosphorylated b_2 (theoretical m/z of 173.1, observed m/z of 173.1) and y_5 (theoretical m/z of 517.3, observed m/z of 517.3) ions, confirms Thr^{535} as the site of phosphorylation. The inset shows the MS spectrum of the doubly charged protonated molecular ion $[M + 2H]^{2+}$. Isotope clusters are separated by 0.505 Da, confirming the charge state of the peptide. (C) Mass spectrum of the 35-residue tryptic peptide ^{657}VADFGLSLLGPVDSGSPLAELPAGTLGYLDPEYYR^{691} supporting a singly phosphorylated residue with a mass of 3731.81 corresponding to the identification of $[M + 2H]^{2+}$ (m/z 1866.81) and $[M + 3H]^{3+}$ (m/z 1244.94) ions.

354.1) and y_6 (theoretical m/z of 698.3, observed m/z of 698.2) ions, along with nonphosphorylated b_2 (theoretical m/z of 173.1, observed m/z of 173.1) and y_5 (theoretical m/z of 517.3, observed m/z of 517.3) ions. Table 2 summarizes the site-determining ions for 16 peptides with confirmed phosphorylation at amino acid residues Ser^{475}, Thr^{478}, Thr^{501}, Ser^{516*}, Ser^{522*}, Thr^{535}, Thr^{536}, Ser^{552}, Thr^{557}, Ser^{563*}, Ser^{644}, Ser^{645}, Thr^{831}, Ser^{837*}, Ser^{875}, and Ser^{888*} (Figure 8A). Five of these confirmed residues, denoted with asterisks, are also found in naïve JKC and represent the basal phosphorylation state of the protein expressed in *E. Coli*. One additional phosphorylation site in the naïve protein is located at either Ser^{811*} or Ser^{812*} in the peptide ^{788}ALAQLMGNPSSEQPILPTEVVLGSSR^{813} (theoretical mass including phosphate group, 2789.34; observed $[M + 3H]^{3+}$, m/z 930.79). Specific y-series ions were obtained showing phosphorylation at the C-terminal end of the peptide, but no site-determining ions were obtained in the fragmentation spectrum to distinguish between the two serine residues.

In addition to these 16 confirmed sites, we identified parent ions with m/z values corresponding to two other peptides, each supporting one phosphorylation site. The peptide ^{852}SSASEGDVAEEEDEGR^{867} (theoretical mass including the phosphate group, m/z 1745.63; observed $[M + 2H]^{2+}$, m/z 873.82) could potentially be phosphorylated at any one of the three serine residues, Ser^{852}, Ser^{853}, or Ser^{855}. However, an exact assignment of the site was not possible because the fragmentation pattern did not reveal the characteristic b- and y-series ions. Similarly, the mass spectrum of the 35-residue tryptic peptide, ^{657}VADFGLSLLGPVDSGSPLAELPAGTLGYLDPEYYR^{691} (Figure 8C) (theoretical mass, including the phosphate group, m/z 3731.81; observed $[M + 3H]^{3+}$, m/z 1244.94), while supporting the presence of one phosphorylated residue among the multiple phosphorylation sites (Ser^{663}, Ser^{670}, Ser^{672}, Thr^{681}, Tyr^{684}, Tyr^{689}, and Tyr^{690}) did not yield the expected set of diagnostic ions in the fragmentation spectrum and hindered a precise localization of the phosphorylated residue. Nevertheless,

dx.doi.org/10.1021/bi101935x |*Biochemistry* 2011, 50, 2170–2186

Table 2. Site-Discriminating Ions for Phosphorylated Residues (red) in Phosphopeptides[a]

Peptide	b ion	Phosphorylated b ion	y ion	Phosphorylated y ion
^{471}SSKDSAFTK^{479}	b4 (+1, 0.14)	b5 (+1, 27.6)	y4 (+1, 1.14)	y5 (+2, 1.62)
^{474}DSAFTKDNGK^{483}	b4 (--)	b5 (+1, 4.9)	y5 (+1, 10.7)	y6 (+2, 2.5)
^{499}VFTYEELEK^{507}	b2 (+1, 6.04)	b3 (+1, 5.77)	y6 (+1, 12.82)	y7 (+1, 22.62)
^{508}AADGFKEESIVGK^{520}	b8 (+1, 0.77)	b9 (+1, 1.07)	y4 (+1, 0.45)	y5 (+1, 0.54)
^{508}AADGFKEESIVGKGSFSCVYK^{528}	b14 (+2, 0.82)	b15 (+2, 3.92)	y6 (+1, 6.07)	y7 (+1, 1.85)
^{533}DGTTVAVK^{540}	b2 (+1, 1.54)	b3 (+1, 1.34)	y5 (+1, 097)	y6 (+2, 2.91)
^{533}DGTTVAVK^{540}	b3 (+1, 2.03)	b4 (--)	y4 (+1, 3.51)	y5 (+1, 1.79)
^{549}QKNSNEFR^{556}	b3 (+1, 0.31)	b4 (--)	y4 (+2, 2.50)	y5 (+2, 1.46)
^{551}NSNEFRTELDLLSR^{564}	b6 (+1, 0.71)	b7 (+1, 2.59)	y7 (+1, 3.33)	y8 (+1, 0.55)
^{557}TELDLLSR^{564}	b6 (+1, 3.16)	b7 (+1, 3.64)	y1 (--)	y2 (--)
^{641}DIKSSNILIDEEHNAR^{656}	b3 (+1, 2.82)	b4 (+1, 2.63)	y12 (+3, 8.75)	y13 (+2, 26.46)
^{641}DIKSSNILIDEEHNAR^{656}	b4 (+1, 3.62)	b5 (--)	y11 (+2, 9.37)	y12 (+2, 6.06)
^{826}SGSENTEFR^{834}	b5 (+1, 2.38)	b6 (+1, 0.42)	y3 (+1, 5.06)	y4 (+1, 5.44)
^{835}GGSWITFPSVTSSQR^{849}	b2 (--)	b3 (--)	y12 (+2, 5.39)	y13 (+2, 4.55)
^{875}SLEEEIGPASPGQSLFLHHNF^{895}	(--)	b1 (--)	y20 (+2, 0.15)	y21 (--)
^{875}SLEEEIGPASPGQSLFLHHNF^{895}	b13 (--)	b14 (+1, 0.32)	y7 (+1, 0.48)	y8 (--)

[a] The percentage of maximal intensity for each site-discriminating ion in the averaged high-resolution CID spectrum is shown in parentheses (supporting ion information available for underlined peptide sequences).

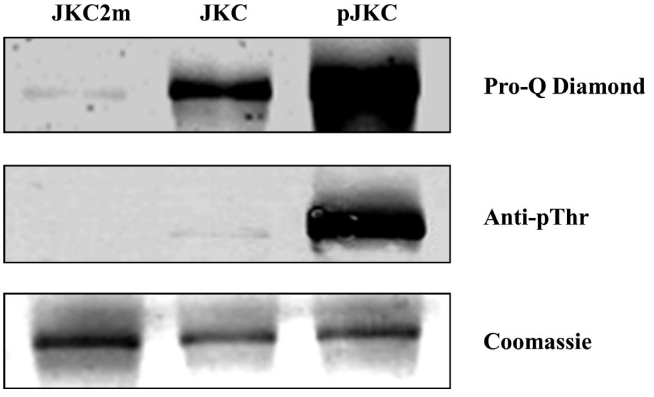

Figure 9. Phosphorylation status of the inactive mutant (JKC2m), naïve JKC (JKC), and the autophosphorylated JKC (pJKC) determined by staining with Pro-Q Diamond (top) and Western blot using the anti-phosphothreonine antibody (middle). The corresponding Coomassie Blue-stained gel of the proteins is shown in the bottom panel.

we were able to narrow the location to either Ser^{670} or Ser^{672} on the basis of a series of y and b ions without a phosphate group. Thus, Thr^{681}, Tyr^{684}, Tyr^{689}, and Tyr^{690} can be eliminated as potential sites on the basis of [M + H] y ions y_5 (m/z 727.341), y_6 (m/z 842.367), y_8 (m/z 1118.513), y_9 (m/z 1175.533), and y_{14} (m/z 1614.782). The m/z values clearly indicate the absence of a phosphate group. Similarly, b ions b_9 (m/z 916.510) and b_{10} (m/z 973.530) do not support Ser^{663} being a phosphorylation site (Figure 8C).

We also assessed the phosphorylation levels of the mutant, naïve, and phosphorylated JKC proteins by staining with Pro-Q Diamond, a phosphospecific stain, and Western blot analysis using the anti-phosphothreonine antibody. Commensurate with data from phosphorylation analysis by mass spectrometry that showed many more phosphorylated residues for the pJKC protein than for the naïve protein, staining with Pro-Q Diamond showed a very intense band for the autophosphorylated protein (pJKC) and a much lower-intensity band for the naïve JKC (Figure 9A). Only a faint band could be seen for the mutant, as would be expected from an inactive protein undergoing little or no phosphorylation. In the Western blot analysis with the anti-phosphothreonine antibody, pJKC exhibited a band of high intensity and the naïve protein barely registered a band (Figure 9B). This correlates well with the observation that all observed phosphorylated sites in the naïve protein are located exclusively on serine residues (Ser^{516*}, Ser^{522*}, Ser^{563*}, Ser ^{811*} or Ser^{812*}, Ser^{837*}, and Ser^{888*}), whereas pJKC has at least six confirmed phosphorylated threonine residues (Thr^{478}, Thr^{501}, Thr^{535}, Thr^{536}, Thr^{557}, and Thr^{831}).

ACR4 RLK Belongs to the RD Family of Kinases. Significantly, the large tryptic peptide ^{657}VADFGLSLLGPVDSGSPLAELPAGTLGYLDPEYYR^{691} also includes the activation loop sequence (the doubly underlined residues between residues DFG and DPE in Figure 8A). It is known that autophosphorylation of specific residue(s) within the activation segment is a critically important regulatory element, and necessary for kinase activity, in many kinases belonging to the Ser/Thr family subgroup (that includes plant kinases and plant RLKs), and the Tyr kinase family subgroup.[33−37] This is a characteristic feature of kinases belonging to the RD family, which contain an Arg residue preceding the invariant catalytic Asp (Figure 10). Crystal structures of RD kinases indicate that phosphorylation in the activation segment promotes a conformational change driven by electrostatic interactions between the negatively charged phosphorylated residue and a cluster of conserved basic residues, including the Arg residue in the RD motif. This conformational

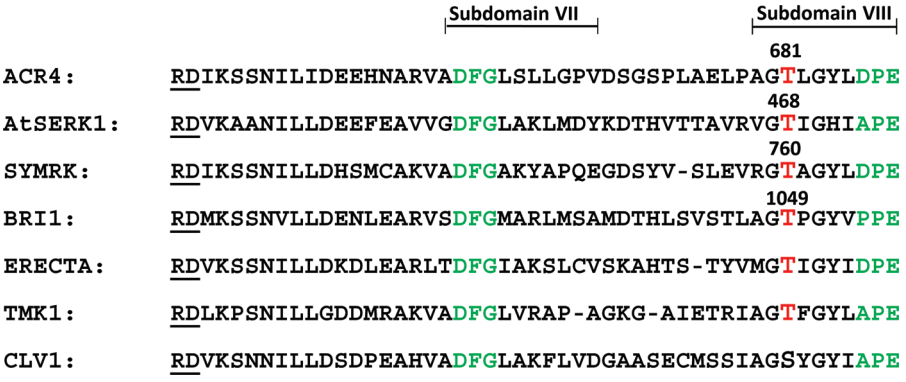

Figure 10. Alignment of the sequences of select RLKs belonging to the RD kinase family showing the Arg residue preceding the invariant Asp in catalytic subdomain VI, the activation loop sequence between "DFG" in subdomain VII and "APE" in subdomain VIII, and the conserved Thr residue. The GenBank accession numbers of the sequences are AB074762 for ACR4, AT4G33430 for AtSERK1/BAK1, AF492655 for SYMRK, AT4G39400 for BRI1, AT2G26330 for ERECTA, AT1G66150 for TMK1, and AT1G75820 for CLV1.

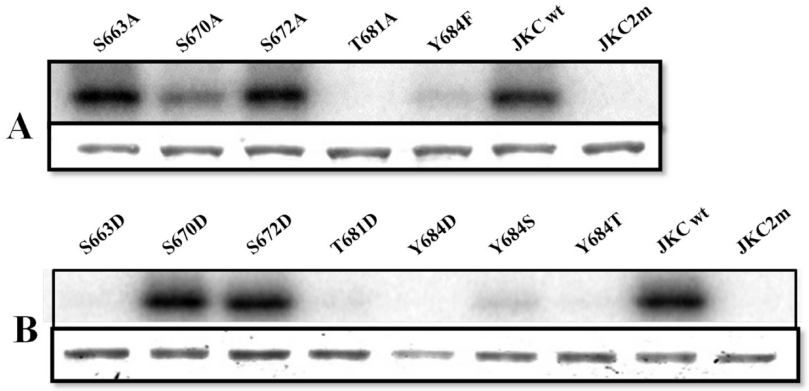

Figure 11. Effect of mutating activation loop phosphorylation sites on kinase activity. (A) Mutations of S^{663}, S^{670}, S^{672}, and T^{681} to Ala and Y^{684} to Phe. (B) Mutations of S^{663}, S^{670}, S^{672}, and T^{681} to Asp and Y^{684} to Asp, Ser, and Thr. Each mutant was purified and subjected to the in vitro kinase assay as described in Materials and Methods. Equal amounts of recombinant proteins were loaded and separated by SDS−PAGE followed by autoradiography. In panels A and B, the top panel shows the autoradiogram and the bottom panel the corresponding Coomassie Blue-stained gel. Wild-type JKC and mutant JKC2m were used as controls.

change reorients the catalytic and substrate binding residues and presents an optimal spatial environment for substrate binding and catalysis. The presence of the RD motif in the ACR4 kinase domain and evidence of phosphorylation of a Ser residue in the activation segment strongly suggest that ACR4 RLK is an RD kinase. To further correlate phosphorylation of the activation loop and kinase activity, we conducted autophosphorylation assays with site-directed mutants in which Ser^{663}, Ser^{670}, Ser^{672}, Thr^{681}, and Tyr^{684} were each replaced separately with either an alanine, which cannot be phosphorylated (Figure 11A), or an aspartic acid (Figure 11B), which mimics phosphorylation. The kinase activity of the S663A mutant was indistinguishable from that of the wild-type protein, but the S663D mutation abolished all activity, suggesting that a negatively charged amino acid was unacceptable at this position but also simultaneously discounting the likely role of Ser^{663} as a substrate. With regard to Ser^{672}, the fact that neither mutation S672A nor mutation S672D changes the kinase activity makes it quite unlikely that it is a favored phosphorylation site. In contrast, the activity of the S670A mutant is significantly knocked down but vigorously restored in the S670D mutant, even though aspartic acid itself is not a substrate for the kinase. This suggests that a negative charge at position 670 is necessary for kinase activity and that this requirement is fulfilled by phosphorylation of Ser^{670}, the most likely candidate residue for phosphorylation. Interestingly, complete loss of autophosphorylation activity is observed when Thr^{681} is mutated to either an alanine or an aspartic acid, indicating that the loss of activity is not linked to the property of the introduced amino acid but is directly attributable to the removal of the Thr residue. Importantly, the fact that even the introduction of a negative charge via an aspartate as a phosphomimetic does not restore kinase activity implicates Thr^{681} as a structurally important residue,[38] in keeping with the tight conservation of this amino acid across a number of RLKs (Figure 10). However, the conserved threonine, Thr^{760}, in the symbiosis receptor kinase, SYMRK,[39] and Thr^{468} in the *Arabidopsis thaliana* somatic embryogenesis receptor-like kinase, *At*SERK1,[40] have also been shown to undergo phosphorylation in vitro. The complete loss of activity seen when Tyr^{684} is replaced with Phe, Asp, Ser, or Thr attests to the importance of non-phosphoamino acid interactions in maintaining the spatial orientations of the activation and catalytic loops in the kinase domain.[38]

Autophosphorylation Induces a Conformational Change. The "conformational plasticity" and structural modifications of kinases in response to phosphorylation and dephosphorylation are well-documented in the literature.[41−43] We have addressed structural perturbations propagated through phosphorylation of

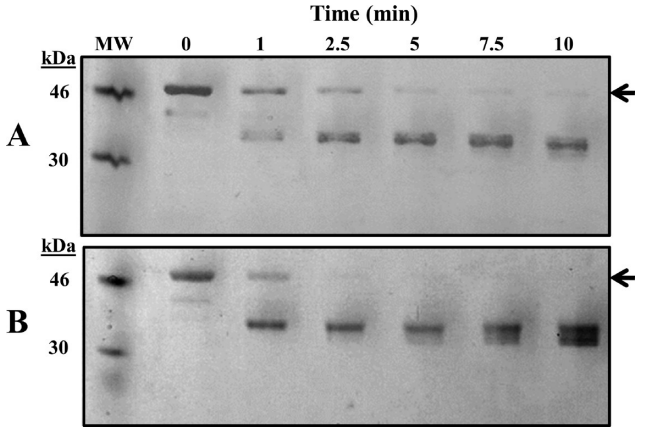

Figure 12. Time course of the tryptic digest of (A) naïve JKC and (B) autophosphorylated pJKC. Proteins were incubated at room temperature for the indicated times with a 1:1000 (w/w) ratio of enzyme to substrate followed by SDS−PAGE analysis. The arrow indicates the mobility of the undigested protein, and molecular weight is the lane with molecular mass markers of 46 and 30 kDa.

the JKC using spectroscopy and limited proteolysis, all techniques that are particularly sensitive to conformational changes in proteins.[44,45] Thus, the CD spectrum of pJKC (16 confirmed phosphorylated residues) in the far-UV region (Figure 3A) is indicative of an alteration in the secondary structure of the protein toward a less compact state in comparison with the naïve form (five confirmed phosphorylated Ser residues) and the mutant protein that is unlikely to contain any phosphorylated residues on the basis of the Pro-Q Diamond staining described earlier. In addition, numerous studies have demonstrated that tryptophan fluorescence in proteins is a sensitive probe of folding and tertiary structure and quite revealing with respect to changes in the microenvironment of aromatic residues.[46,47] In comparison with the fluorescence spectra of naïve JKC and the JKC2m mutant (Figure 3B), the intensity of the intrinsic tryptophan fluorescence of the pJKC was observed to decrease significantly, accompanied by a blue shift in the λ_{max} of emission (from 342 to 338 nm) and the appearance of a shoulder at 310 nm, which can be attributed to tyrosine fluorescence. Limited proteolysis is also a well-established technique for probing protein conformation and dynamics and relies on the fact that proteolysis occurs at sites with enhanced local flexibility.[48−50] Well-folded regions within proteins usually resist protease digestion, and therefore, the protected fragments remaining after trypsin digestion represent stably folded domains. The digestion patterns of naïve JKC and pJKC with trypsin as a function of time (Figure 12) provide additional evidence of phosphorylation-induced conformational change. Whereas with naïve JKC, undigested protein could be detected during incubation with trypsin for the first 10 min (Figure 12A), there was little evidence of undigested protein in the case of pJKC after the first 2.5−5 min (Figure 12B), and there was significantly faster accumulation of the ∼37 kDa protein, presumably the kinase domain, as indicated by Western blot analysis (data not shown).

DISCUSSION

In this study, we have demonstrated that the ACR4 intracellular domain encodes a functional kinase that undergoes autophosphorylation on 16 confirmed sites, two of which occur in the juxtamembrane domain, 10 in the kinase domain, and four in the carboxy-terminal domain. However, as noted earlier, there is evidence of three other unconfirmed phosphorylation sites. Because of substoichiometric representation of phosphopeptides, it is quite likely that additional phosphorylated residues may have gone undetected in our LC−MS/MS analysis. Regulation of kinase activity and recruitment of downstream interacting proteins via multiple sites of phosphorylation are common features of animal RTKs, as exemplified by EGFR.[5,6,51] Their occurrence in many plant RLKs[52] suggests a conserved mechanism of control of signal transduction processes across the two kingdoms. In the RTKs, for example, phosphorylated residues in the juxtamembrane and carboxy-terminal regions not only serve a regulatory role[41,53] but act as docking sites for specific signaling molecules such as those containing Src homology 2 (SH2) domains or phosphotyrosine-binding (PTB) domains.[54−56] Phosphorylation of Ser/Thr residues also creates binding surfaces for diverse phosphoamino acid binding modules such as the 14-3-3, WW, and forkhead-associated (FHA) modules.[57,58] The 14-3-3 modules are well represented in the *Arabidopsis* genome.[59−61] An example of an FHA-containing module in *Arabidopsis* is the kinase-associated protein phosphatase (KAPP). KAPP binds to phosphorylated Ser/Thr residues of several plant RLKs such as CLAVATA 1 (CLV1), SERK1, HAESA, and FLS2 and acts as a negative regulator of receptor signaling.[62−65] The phosphorylated Ser and Thr residues in the ACR4 juxtamembrane and carboxy-terminal domains of ACR4 could very well serve as docking sites for similar interacting proteins.

Many protein kinases also achieve maximal enzymatic activity only after phosphorylation of specific residues in the activation loop sequence that occurs between subdomains VII and VIII of the kinase domain.[66] In some RD kinases among plant RLKs, activation loop phosphorylation is essential for both autophosphorylation and substrate phosphorylation. Thus, in BRI1, the T1049A mutation abolishes autophosphorylation and substrate phosphorylation in vitro, and the mutant is also unable to rescue the weak *bri1-5* Brassinolide insensitive mutant in planta.[37] In the activation segment sequence alignment, the correspondingly conserved residue in SYMRK (Thr^{760}) is phosphorylated in vitro and the Ala mutant has little or no autophosphorylation or substrate phosphorylation activity.[39] Similarly, the conserved Thr^{468} in AtSERK1 is important for both autophosphorylation and phosphorylation of artificial substrates in vitro.[36] The strict conservation of Thr at this position in the activation segment of RD-type RLKs (Figure 10) suggests that it may be an important in vivo phosphorylation site. In ACR4, the equivalent residue, Thr^{681}, does not appear to be phosphorylated by LC−MS/MS analysis, but our mutagenesis experiments clearly demonstrate that it is required for in vitro kinase activity. This result, however, does not preclude the possibility of Thr^{681} being phosphorylated in vivo. Importantly, as in the case of BRI1, SYMRK, and AtSERK1, additional phosphorylation sites within the activation segment of RD-type RLKs that are not conserved in the sequence alignment appear to be required for activation and function. Presumably, multiple phosphorylations induce conformational changes that regulate binding sites for ATP and other substrates.[67] Intriguingly, in addition to regulating kinase activity, phosphorylations in the activation segment can also facilitate recruitment of downstream partners, as in the case of the interaction between the SH2 domain of the adaptor protein APS and the phosphotyrosines in the activation loop of the

insulin receptor kinase.[68,69] In another interesting example, in the extracellular signal-regulated kinase (ERK), phosphorylation-dependent conformational changes in the activation loop affect the subcellular localization of the protein.[70]

It appears likely that autophosphorylation-induced conformational changes also affect the gross structure of the intracellular domain. Thus, molecular interactions within the JKC, involving both the juxtamembrane and carboxy-terminal domains, could hold the molecule in a "closed" conformation, and the release of these interactions upon phosphorylation results in a more "open" conformation. Some support for this comes from the limited proteolysis experiment that shows a relatively faster accumulation of the 37 kDa kinase domain after phosphorylation. Indeed, in the case of BRI1, the carboxy-terminal region negatively regulates BRI1 function, and deletion of this region enhances kinase activity.[71] Even in RTKs, regions proximal to the catalytic domain are known to play vital roles in kinase activation mechanisms. In several receptors such as those of the ephrin binding receptor (EpH) family, platelet-derived growth factor (PDGF) receptor family, and epidermal growth factor receptor (EGFR) family, the juxtamembrane domain is a major regulatory domain.[72−75] Similarly, the domain on the carboxyl side of the kinase domain can be autoinhibitory, which has been demonstrated for EGFR and the receptor TIE2, an RTK that is activated by angiopoietin-1.[76,77]

The classical paradigm of receptor kinase function invokes ligand binding, followed by dimerization of the receptor, concomitant conformational change, and activation of the kinase domain by cis (intramolecular) or trans (intermolecular) autophosphorylation.[1,2] The ligand for ACR4 is as yet unknown, but here we report that the autophosphorylation of NusA:JKC occurs through an intramolecular mechanism, a property associated with similar domains from RLKs such as XA21 that is involved in rice disease resistance,[78] BRI1 (Brassinosteroid Insensitive 1) that is an essential receptor controlling plant development,[31] and CrRLK1 from the plant *Cantharanthus roseus*.[30] This would suggest that ligand-mediated dimerization may not be essential for activation of kinase activity. However, in vivo, alternative modes of activation remain distinctly viable. It is conceivable that ligand binding to the extracellular domain of ACR4 induces a conformational change in its intracellular domain that allows subsequent interaction with a second kinase (membrane-bound or soluble) that is capable of trans phosphorylating at a specific site on the ACR4 intracellular domain and "activating" an intramolecular autophosphorylation event. In *Arabidopsis*, candidate proteins that could be involved in such interactions include the CRINKLY4-related (CRR) proteins[13] and the receptor-like kinase, ABNORMAL LEAF SHAPE 2 (ALE2).[79] The four CRR proteins found in *Arabidopsis* (AtCRR1, AtCRR2, AtCRR3, and AtCRK1) share similar structural features with ACR4, but only AtCRK1 encodes a kinase domain with phosphorylation activity in an in vitro assay.[13] It is possible that receptor activation and autophosphorylation of ACR4 kinase could be stimulated by heteromeric interactions with the AtCRR proteins. Evidence of the involvement of ACR4 and the AtCRRs in a common signal transduction pathway, perhaps mediated by heterodimerization, comes from the observation that, in vitro, the ACR4 kinase domain can phosphorylate the inactive kinase domain of AtCRR2.[13] Similarly, genetic studies indicate that pathways involving ALE2 and ACR4 might act positively to regulate the specification of the protoderm and/or protoderm specific genes in the formation of leafy organs.[79] Intriguingly, in in vitro experiments, the kinase domains of ACR4 and ALE2 can also phosphorylate each other.[79]

Our experiments suggest that the intracellular domain of ACR4 possesses an intrinsic propensity to form higher-order oligomers, although the precise contributions of the JM region and the CTD remain to be ascertained in future experiments. The fact that the NusA protein itself does not dimerize rules out the possibility of any influence of the NusA tag on the oligomerization of the JKC. The significance of this observation in the context of ACR4 function remains to be established in more detailed molecular studies both in vitro and in vivo. In animals, in addition to ligand-induced dimerization, RTKs such as NGFR, EGFR, and the erythropoietin receptor can exist as preformed dimers even in the absence of ligand.[80−84] Furthermore, in the case of EGFR, the juxtamembrane domain is required for dimerization of the cytoplasmic domain.[85] Among RLKs, BRI1[86−88] and the S-locus receptor kinase[89] have been shown to exist as ligand-independent dimers, but structural features contributing to the dimerization process are unknown. The precise mechanism of productive oligomer formation and activation among plant RLKs is not completely understood and could vary among the receptor subclasses. However, in the case of BRI1, biochemical and genetic evidence of a model in which ligand binding activates a preexisiting BRI1 dimer that then associates with the coreceptor BAK1 and transphosphorylates key residues in the kinase domain has been provided, followed by reciprocal transphosphorylation of BRI1 by the activated BAK1.[90]

The sedimentation velocity experiments also demonstrate that autophosphorylation of NusA:JKC prevents oligomerization, which perhaps can be attributed to electrostatic repulsions between negatively charged phosphorylated residues on the protein. However, the large size of the NusA tag, and the fact that it also is phosphorylated, precludes an unambiguous interpretation of the precise effect of autophosphorylation on the association−dissociation properties of the intracellular domain.

In conclusion, in this study, we describe for the first time the biochemical properties of the intracellular domain of ACR4 and provide key insights into its phosphorylation kinetics. Ongoing and future experiments in our laboratory will address more detailed molecular analyses to delineate the role of the subdomains in ACR4 structure and function, interactions with putative partners, and mutational analysis of phosphorylation sites. Mutating different phosphorylation sites within ACR4 could have strikingly different effects, including changes in receptor function, changes in receptor stability and/or turnover, and changes in subcellular localization. Clearly, the identification of the physiological substrates of the kinase and in vivo phosphorylation sites is essential to understanding the signaling pathway mediated by ACR4. Our in vitro studies will complement genetic approaches and contribute to an overall understanding of ACR4 function in plants.

AUTHOR INFORMATION

Corresponding Author

*Department of Biochemistry, Biophysics and Molecular Biology, Iowa State University, Ames, IA 50011. Phone: (515) 294-6116. Fax: (515) 294-0453. E-mail: gururao@iastate.edu.

Funding Sources

This research was supported by startup funding from Iowa State University to A.G.R., in part by Grants P41 RR000954 and Ul1

RR024992 from the National Center for Research Resources, part of the National Institutes of Health (NIH), and by the NIH Roadmap for Medical Research (R.R.T.).

■ ACKNOWLEDGMENT

We thank Prof. Alan DiSpirito and Dr. Raji Joseph of the Department of Biochemistry, Biophysics and Molecular Biology and Dr. Suman Kundu (Department of Biochemistry, University of Delhi, New Delhi, India) for their critical reading of the manuscript. The expert technical assistance of Petra Erdmann-Gilmore and Alan E. Davis is gratefully acknowledged.

■ ABBREVIATIONS

ACR4, *Arabidopsis* CRINKLY4; ALE2, Abnormal Leaf Shape 2; BRI1, Brassinosteroid insensitive 1; CR4, maize CRINKLY4; CD, circular dichroism; AtCRR, *Arabidopsis* CRINKLY4-related; CTD, carboxy-terminal domain; DTT, dithiothreitol; EGFR, epidermal growth factor receptor; ICD, intracellular domain; JKC, juxtamembrane + kinase + carboxy-terminal domain; pJKC, phosphorylated JKC; JM, juxtamembrane; KD, kinase domain; MyBP, myelin basic protein; NusA, N-utilization substance A; PDGF, platelet-derived growth factor; RLK, receptor-like kinase; RTK, receptor tyrosine kinase; SERK, somatic embryogenesis receptor-like kinase; SYMRK, symbiosis receptor kinase; TCEP, tris(2-carboxyethyl)phosphine hydrochloride; UV, ultraviolet.

■ REFERENCES

(1) Jiang, G., and Hunter, T. (1999) Receptor activation: When a dimer is not enough. *Curr. Biol. 9*, R568–R571.

(2) Schlessinger, J. (2000) Cell signaling by receptor tyrosine kinases. *Cell 103*, 211–225.

(3) Olayiye, M., Neve, R. M., Lane, H. A., and Hynes, N. E. (2000) The ErbB signaling network: Receptor heterodimerization in development and cancer. *EMBO J. 19*, 3159–3167.

(4) Schlessinger, J. (2002) Ligand-induced, receptor-mediated dimerization and activation of EGF receptor. *Cell 110*, 669–672.

(5) Schulze, W. X., Deng, L., and Mann, M. (2005) Phosphotyrosine interactome of the ErbB-receptor kinase family. *Mol. Syst. Biol. 1*, No. 2005.0008.

(6) Jones, R. B., Gordus, A., Krall, J. A., and MacBeath, G. (2006) A quantitative protein interaction network for the ErbB receptors using protein microarrays. *Nature 439*, 168–174.

(7) Holbro, T., and Hynes, N. E. (2004) ErbB receptors: Directing key signaling networks throughout life. *Annu. Rev. Pharmacol. Toxicol. 44*, 195–217.

(8) Wieduwilt, M. J., and Moasser, M. M. (2008) The epidermal growth factor receptor family: Biology driving targeted therapeutics. *Cell. Mol. Life Sci. 65*, 1566–1584.

(9) Shiu, S.-H., and Bleecker, A. B. (2001) Plant receptor-like kinase gene family: Diversity, function and signaling. *Sci. STKE 2001*, No. re22.

(10) Heffani, Y. Z., Silva, N. F., and Goring, D. R. (2004) Receptor kinase signaling in plants. *Can. J. Bot. 82*, 1–15.

(11) Becraft, P. W., Stinard, P. S., and McCarty, D. R. (1996) CRINKLY4: A TNFR-like receptor kinase involved in maize epidermal differentiation. *Science 273*, 1406–1409.

(12) Jin, P., Guo, T., and Becraft, P. W. (2000) The maize CR4 receptor-like kinase mediates a growth factor-like differentiation response. *Genesis 27*, 104–116.

(13) Cao, X., Li, K., Suh, S.-G., Guo, T., and Becraft, P. W. (2005) Molecular analysis of the CRINKLY4 gene family in *Arabidopsis thaliana*. *Planta 220*, 645–657.

(14) Gifford, M. L., Robertson, F. C., Soares, D. C., and Ingram, G. C. (2005) *Arabidopsis* CRINKLY4 function, internalization and turnover are dependent on the extracellular crinkly repeat domain. *Plant Cell 17*, 1154–1166.

(15) Tanaka, H., Watanabe, M., Watanabe, D., Tanaka, T., Machida, C., and Machida, Y. (2002) ACR4, a putative receptor kinase gene of *Arabidopsis thaliana*, that is expressed in the outer cell layers of embryos and plants, is involved in proper embryogenesis. *Plant Cell Physiol. 43*, 419–428.

(16) Gifford, M. L., Dean, S., and Ingram, G. C. (2003) The *Arabidopsis* ACR4 gene plays a role in cell layer organization during ovule integument and sepal margin development. *Development 130*, 4249–4258.

(17) Watanabe, M., Tanaka, H., Watanabe, D., Machida, C., and Machida, Y. (2004) The ACR4 receptor-like kinase is required for surface formation of epidermis-related tissues in *Arabidopsis thaliana*. *Plant J. 39*, 298–308.

(18) De Smet, I., Vassileva, V., De Rybel, B., Levesque, M. P., Grunewald, W., Van Damme, D., Van Noorden, G., Naudts, M., Van Isterdael, G., De Clercq, R., Wang, J. Y., Meuli, N., Vanneste, S., Friml, J., Hilson, P., Jürgens, G., Ingram, G. C., Inzé, D., Benfey, P. N., and Beeckman, T. (2008) Receptor-like kinase ACR4 restricts formative cell divisions in the *Arabidopsis* root. *Science 322*, 594–597.

(19) Stahl, Y., Wink, R. H., Ingram, G. C., and Simon, R. (2009) A signaling module controlling the stem cell niche in *Arabidopsis* root meristems. *Curr. Biol. 19*, 909–914.

(20) Nittis, T., Guittat, L., LeDuc, R. D., Dao, B., Duxin, J. P., Rohrs, H., Townsend, R. R., and Stewart, S. A. (2010) Revealing novel telomere proteins using In Vivo cross-linking, tandem affinity purification, and label-free quantitative LC-FTICR-MS. *Mol. Cell. Proteomics 9*, 1144–1156.

(21) Van Holde, K. E., and Weischet, W. O. (1978) Boundary analysis of sedimentation velocity experiments with monodisperse and paucidisperse solutes. *Biopolymers 17*, 1387–1403.

(22) Wente, S. R., Villalba, M., Schramm, V., and Rosen, O. M. (1990) Mn^{2+}-binding properties of a recombinant protein-tyrosine kinase derived from the human insulin receptor. *Proc. Natl. Acad. Sci. U.S.A. 87*, 2805–2809.

(23) Sierke, S. L., Cheng, K., Kim, H. H., and Koland, J. G. (1997) Biochemical characterization of the protein tyrosine kinase homology domain of the ErbB3 (HER3) receptor protein. *Biochem. J. 322*, 757–763.

(24) Hansen, J. C., Lebowitz, J., and Demeler, B. (1994) Analytical ultracentrifugation of complex macromolecular systems. *Biochemistry 33*, 13155–13163.

(25) Gill, S. C., Weitzel, S. E., and von Hippel, P. H. (1991) *Escherichia coli* sigma 70 and NusA proteins. I. Binding interactions with core RNA polymerase in solution and within the transcription complex. *J. Mol. Biol. 220*, 307–324.

(26) Gill, S. C., Weitzel, S. E., and von Hippel, P. H. (1991) *Escherichia coli* sigma 70 and NusA proteins. II. Physical properties and self-association states. *J. Mol. Biol. 220*, 325–333.

(27) Shin, D. H., Nguyen, H. H., Jancarik, J., Yokota, H., Kim, R., and Kim, S.-H. (2003) Crystal Structure of NusA from *Thermotoga maritima* and Functional Implication of the N-Terminal Domain. *Biochemistry 42*, 13429–13437.

(28) Gopal, B., Haire, L. F., Gamblin, S. J., Dodson, E. J., Lane, A. N., Papavinasasundaram, K. G., Colston, M. J., and Dodson, G. (2001) Crystal structure of the transcription elongation/anti-termination factor NusA from *Mycobacterium tuberculosis* at 1.7 Å resolution. *J. Mol. Biol. 314*, 1087–1095.

(29) Horn, M. A., and Walker, J. C. (1994) Biochemical properties of the autophosphorylation of RLK5, a receptor-like protein kinase from *Arabidopsis thaliana*. *Biochim. Biophys. Acta 1208*, 65–74.

(30) Schulze-Muth, P., Irmler, S., Schroder, G., and Schroder, J. (1996) Novel type of receptor-like protein kinase from a higher plant (*Catharanthus roseus*). cDNA, gene, intramolecular autophosphorylation, and identification of a threonine important for auto- and substrate phosphorylation. *J. Biol. Chem. 271*, 26684–26689.

(31) Oh, M. H., Ray, W. K., Huber, S. C., Asara, J. M., Gage, D. A., and Clouse, S. D. (2000) Recombinant brassinosteroid insensitive 1 receptor-like kinase autophosphorylates on serine and threonine residues and phosphorylates a conserved peptide motif *in vitro*. *Plant Physiol. 124*, 751–766.

(32) Beausoleil, S. A., Villen, J., Gerber, S. A., Rush, J., and Gygi, S. P. (2006) A probability based approach for high-throughput protein phosphorylation analysis and site localization. *Nat. Biotechnol. 24*, 1485.

(33) Johnson, L. N., Noble, M. E. M., and Owen, D. J. (1996) Active and inactive protein kinases: Structural basis for regulation. *Cell 85*, 149–158.

(34) Johnson, L. N., and Lewis, R. J. (2001) Structural basis for control by phosphorylation. *Chem. Rev. 101*, 2209–2242.

(35) Burza, A. M., Pekala, I., Sikora, J., Siedlecki, P., Malagocki, P., Bucholc, M., Koper, L., Zielenkiewicz, P., Dadlez, M., and Dobrowolska, G. (2006) *Nicotiana tobaccum* osmotic stress-activated kinase is regulated by phosphorylation on Ser-154 and Ser-158 in the kinase activation loop. *J. Biol. Chem. 281*, 34299–34311.

(36) Shah, K., Vervoort, J., and de Vries, S. C. (2001) Role of threonines in the Arabidopsis *thaliana* somatic embryogenesis receptor kinase 1 activation loop in phosphorylation. *J. Biol. Chem. 276*, 41263–41269.

(37) Wang, X., Goshe, M. B., Soderblom, E. J., Phinney, B. S., Kushar, J. A., Li, J., Asami, T., Yoshida, S., Huber, S. C., and Clouse, S. D. (2005) Identification and functional analysis of In Vivo phosphorylation sites of the *Arabidopsis* BRASSINOSTEROID-INSENSITIVE 1 receptor kinase. *Plant Cell 17*, 1685–1703.

(38) Krupa, A., Preethi, G., and Srinivasan, N. (2004) Structural modes of stabilization of permissive phoshphorylation sites in protein kinases: Distinct strategies in Ser/Thr and Tyr kinases. *J. Mol. Biol. 339*, 1025–1039.

(39) Yoshida, S., and Parniske, M. (2005) Regulation of plant symbiosis receptor kinase through serine and threonine phosphorylation. *J. Biol. Chem. 280*, 9203–9209.

(40) Karlova, R., Boeren, S., van Dongen, W., Kwaaitaal, M., Aker, J., Vervoort, J., and de Vries, S. (2009) Identification of in vitro phosphorylation sites in the *Arabidopsis thaliana* somatic embryogenesis receptor-like kinases. *Proteomics 9*, 368–379.

(41) Huse, M., and Kuriyan, J. (2002) The conformational plasticity of protein kinases. *Cell 109*, 275–282.

(42) Nolan, B., Taylor, S., and Ghosh, G. (2004) Regulation of protein kinases: Controlling activity through activation segment conformation. *Mol. Cell 15*, 661–675.

(43) Groban, E. S., Narayanan, A., and Jacobson, M. P. (2006) Conformational changes in protein loops and helices induced by post-translational phosphorylation. *PLoS Comput. Biol. 2* (4), No. e32.

(44) Roesler, K. R., and Rao, A. G. (1999) Conformation and stability of barley chymotrypsin inhibitor-2 (CI-2) mutants containing multiple lysine substitutions. *Protein Eng. 12*, 967–973.

(45) Roesler, K. R., and Rao, A. G. (2000) A single disulfide bond restores thermodynamic and proteolytic stability to an extensively mutated protein. *Protein Sci. 9*, 1642–1650.

(46) Laskowicz, J. R. (1983) in *Principles of Fluorescence Spectroscopy*, Plenum Press, New York.

(47) Barry, J. K., Selinger, D. A., Wang, C., Olsen, O.-A., and Rao, A. G. (2006) Biochemical characterization of a truncated penta-EF-hand Ca^{2+} binding protein from maize. *Biochim. Biophys. Acta 1764*, 239–245.

(48) Fontana, A., Fassina, G., Vita, C., Dalzoppo, D., Zamai, M., and Zambonin, M. (1986) Correlation between sites of limited proteolysis and segmental mobility in thermolysin. *Biochemistry 25*, 1847–1851.

(49) Polverino, P., Frare, E., Gottardo, R., Dael, V. H., and Fontana, A. (2002) Partly folded states of members of the lysozyme/lactalbumin superfamily: A comparative study by circular dichrosim spectroscopy and limited proteolysis. *Protein Sci. 11*, 2932–2946.

(50) Kamath, N., Karwowska-Desaulniers, P., and Pflum, M. K. H. (2006) Limited proteolysis of human histone deacetylase 1. *BMC Biochem. 7*, 22–36.

(51) Lemmon, M. A., and Schlessinger, J. (2010) Cell signaling by receptor tyrosine kinases. *Cell 141*, 1117–1134.

(52) Nuhse, T. S., Stensballe, A., Jensen, O. N., and Peck, S. C. (2004) Phosphoproteomics of the *Arabidopsis* plasma membrane and a new phosphorylation site database. *Plant Cell 16*, 2394–2405.

(53) Adams, J. A. (2003) Activation loop phosphorylation and catalysis in protein kinases: Is there functional evidence for the autoinhibitor model?. *Biochemistry 42*, 601–607.

(54) Yarden, Y., and Sliwkowski, M. X. (2001) Untangling the ErbB signaling network. *Nat. Rev. Mol. Cell Biol. 2*, 127–137.

(55) Pawson, T., and Nash, P. (2000) Protein-protein interactions define specificity in signal transduction. *Genes Dev. 14*, 1027–1047.

(56) Herbst, R., and Burden, S. J. (2000) The juxtamembrane region of MuSK has a critical role in agrin-mediated signaling. *EMBO J. 19*, 67–77.

(57) Yaffe, M. B., and Elia, A. E. (2001) Phosphoserine/threonine-binding domains. *Curr. Opin. Cell Biol. 13*, 131–138.

(58) Li, J., Lee, G.-I., Van Doren, S. R., and Walker, J. C. (2000) The FHA domain mediates phosphoprotein interactions. *J. Cell Sci. 113*, 4143–4149.

(59) DeLille, J., Sehnke, P. C., and Ferl, R. J. (2001) The *Arabidopsis thaliana* 14-3-3 family of signaling regulators. *Plant Physiol. 126*, 35–38.

(60) Rosenquist, M., Alsterfjord, M., Larsson, C., and Sommarin, M. (2001) Data mining the *Arabidopsis* genome reveals fifteen 14-3-3 genes. Expression is demonstrated for two out of five novel genes. *Plant Physiol. 127*, 142–149.

(61) Sehnke, P. C., DeLille, J. M., and Ferl, R. J. (2002) Consummating signal transduction: The role of 14-3-3 proteins in the completion of signal-induced transitions in protein activity. *Plant Cell* S339–S354.

(62) Williams, R. W., Wilson, J. M., and Meyerowitz, E. M. (1997) A possible role for kinase-associated protein phosphatase in the *Arabidopsis* CLAVATA1 signaling pathway. *Proc. Natl. Acad. Sci. U.S.A. 94*, 10467–10472.

(63) Shah, K., Russinova, E., Gadella, T. W., Jr., Willemse, J., and De Vries, S. C. (2002) The *Arabidopsis* kinase- associated protein phosphatase controls internalization of the somatic embryogenesis receptor kinase 1. *Genes Dev. 16*, 1707–1720.

(64) Stone, J. M., Colinge, M. A., Smith, R. D., Horn, M. A., and Walker, J. C. (1994) Interaction of a protein phosphatase with an *Arabidopsis* serine-threonine receptor kinase. *Science 266*, 793–795.

(65) Gomez-Gomez, L., Bauer, Z., and Boller, T. (2001) Both the extracellular leucine-rich repeat domain and the kinase activity of FLS2 are required for flagellin binding and signaling in *Arabidopsis*. *Plant Cell 13*, 1155–1163.

(66) Hanks, S. K., and Hunter, T. (1995) Protein kinases 6. The eukaryotic protein kinase superfamily: Kinase (catalytic) domain structure and classification. *FASEB J. 9*, 576–596.

(67) Hubbard, S. R. (1997) Crystal structure of the activated insulin receptor tyrosine kinase in complex with peptide substrate and ATP analog. *EMBO J. 16*, 5572–5581.

(68) Moodie, S. A., Alleman-Sposeto, J., and Gustafson, T. A. (1999) Identification of the APS protein as a novel insulin receptor substrate. *J. Biol. Chem. 274*, 11186–11193.

(69) Hu, J., Liu, J., Ghirlando, R., Saltiel, A. R., and Hubbard, S. R. (2003) Structural basis for recruitment of the adaptor protein APS to the activated insulin receptor. *Mol. Cell 12*, 1379–1389.

(70) Wolf, I., Rubenfeld, H., Yoon, S., Marmor, G., Hanoch, T., and Seger, R. (2001) Involvement of the activation loop of ERK in the detachment from cytosolic anchoring. *J. Biol. Chem. 276*, 24490–24497.

(71) Wang, X., Li, X., Meisenhelder, J., Junter, T., Yoshida, S., Asami, T., and Chory, J. (2005) Autoregulation and homodimerization are involved in the activation of the plant steroid receptor BRI1. *Dev. Cell 8*, 855–865.

(72) Wybenga-Groot, L. E., Baskin, B., Ong, S. H., Tong, J., Pawson, T., and Sicheri, F. (2001) Structural basis for autoinhibition of the EphB2 receptor tyrosine kinase by the naive juxtamembrane region. *Cell 106*, 745–757.

(73) Griffith, J., Black, J., Faermon, C., Swenson, L., Wynn, M., Lu, F., Lipke, J., and Saxena, K. (2004) The structural basis for autoinhibition of FLT3 by the juxtamembrane domain. *Mol. Cell 13*, 169–178.

(74) Thiel, K. W., and Carpenter, G. (2007) Epidermal growth factor receptor juxtamembrane region regulates allosteric tyrosine kinase activation. *Proc. Natl. Acad. Sci. U.S.A. 104*, 19238–19243.

(75) Hubbard, S. R. (2004) Juxtamembrane autoinhibition in receptor tyrosine kinases. *Nat. Rev. Mol. Cell Biol. 5*, 464–470.

(76) Lee, N. Y., and Koland, J. G. (2005) Conformational changes accompany phosphorylation of the epidermal growth factor receptor C-terminal domain. *Protein Sci. 14*, 2793–2803.

(77) Niu, X. L., Peters, K. G., and Kontos, C. D. (2002) Deletion of the carboxy terminus of Tie2 enhances kinase activity, signaling and function: Evidence for an autoinhibitory mechanism. *J. Biol. Chem. 277*, 31768–31773.

(78) Liu, G.-Z., Pi, L.-Y., Walker, J. C., Ronald, P. C., and Song, W.-Y. (2002) Biochemical characterization of the kinase domain of the rice disease resistance receptor-like kinase XA21. *J. Biol. Chem. 277*, 20264–20269.

(79) Tanaka, H., Watanabe, M., Sasabe, M., Hiroe, T., Tanaka, T., Tsukuya, H., Ikezaki, M., Machida, C., and Machida, Y. (2007) Novel receptor-like kinase ALE2 controls shoot development by specifying epidermis in *Arabidopsis*. *Development 134*, 1643–1652.

(80) Gadella, T. W. J., Jr., and Jovin, T. M. (1995) Oligomerization of epidermal growth factor receptors on A431 cells studied by time-resolved fluorescence imaging microscopy. A stereochemical model for tyrosine kinase receptor activation. *J. Cell Biol. 129*, 1543–1558.

(81) Livnah, O., Stura, F. A., Middleton, S. A., Johnson, D. L., Jolliffe, I. K., and Wilson, I. A. (1999) Crystallographic evidence for preformed dimers of erythropoietin receptor before ligand activation. *Science 283*, 987–990.

(82) Moriki, T., Maruyama, H., and Maruyama, I. N. (2001) Activation of preformed EGF receptor dimers by ligand induced rotation of the transmembrane domain. *J. Mol. Biol. 311*, 1011–1026.

(83) Mischel, P. S., Umbach, J. A., Eskandari, S., Smith, S. G., Gunderson, C. B., and Zamphigi, G. A. (2002) Nerve growth factor signals via preexisting TrkA receptor oligomers. *Biophys. J. 83*, 968–976.

(84) Ferguson, K. M., Berger, M. B., Mendrola, J. M., Cho, H. S., Leahy, D. J., and Lemmon, M. A. (2003) EGF activates its receptor by removing interactions that autoinhibit ectodomain dimerization. *Mol. Cell 11*, 507–517.

(85) Aifa, S., Aydin, J., Nordvall, G., Lundtrom, I., Svensson, S. P. S., and Hermanson, O. (2005) A basic peptide within the juxtamembrane region is required for EGF receptor dimerization. *Exp. Cell Res. 302*, 108–114.

(86) Russinova, E., Borst, J.-W., Kwaaitaal, M., Cano-Delgado, A., Yin, Y., Chory, J., and de Vries, S. C. (2004) Heterodimerization and endocytosis of *Arabidopsis* brassinosteroid receptors BRI1 and AtSERK3 (BAK1). *Plant Cell 16*, 3216–3229.

(87) Wang, X., Goshe, M. B., Soderblom, E. J., Phinney, B. S., Kuchar, J. A., Li, J., Asami, T., Yoshida, S., Huber, S. C., and Clouse, S. D. (2005) Identification and functional analysis of *In Vivo* phosphorylation sites of the *Arabidopsis* Brassinosteroid-Insensitive1 receptor kinase. *Plant Cell 17*, 1685–1703.

(88) Hink, M. A., Shah, K., Russinova, E., de Vries, S. C., and Vissar, A. J. (2008) Fluorescence fluctuation analysis of *Arabidopsis thaliana* somatic embryogenesis receptor-like kinase and brassinosteroid insensitive 1 receptor oligomerization. *Biophys. J. 94*, 1052–1062.

(89) Giranton, J. L., Dumas, C., Cock, J. M., and Gaude, T. (2000) The integral membrane S-locus receptor kinase of *Brassica* has serine/threonine kinase activity in a membranous environment and spontaneously forms oligomers in planta. *Proc. Natl. Acad. Sci. U.S.A. 97*, 3759–3764.

(90) Wang, X., Kota, U., He, K., Blackburn, K., Li, J., Goshe, M. B., Huber, S. C., and Clouse, S. D. (2008) Sequential transphosphorylation of the BRI1/BAK1 receptor kinase complex impacts early events in brassinosteroid signaling. *Dev. Cell 15*, 220–235.